

# Supporting Deterministic Traffic on Standard NICs

Chuanyu Xue  
University of Connecticut  
chuanyu.xue@uconn.edu

Tianyu Zhang  
University of Iowa  
tianyu-zhang@uiowa.edu

Andrew Loveless  
NASA JSC  
andrew.loveless@nasa.gov

Song Han  
University of Connecticut  
song.han@uconn.edu

## Abstract

Networked mission-critical applications (e.g., avionic control and industrial automation systems) require deterministic packet transmissions to support a range of sensing and control tasks with stringent timing constraints. While specialized network infrastructure (e.g., time-sensitive networking (TSN) switches) provides deterministic data transport across the network, achieving strict end-to-end timing guarantees requires equally capable end devices to support deterministic traffic. These end devices, however, often employ general-purpose computing platforms like standard PCs, which lack native support for deterministic traffic and suffer from unpredictable delays introduced by their software stack and system architecture. Although specialized NICs with hardware scheduling offload can mitigate this problem, the limited compatibility hinders their widespread adoption, particularly for cost-sensitive applications or in legacy devices.

To fill this gap, this paper proposes a novel software-based driver model, namely KeepON, to enable the support of deterministic packet transmissions on end devices equipped with standard NICs. The key idea of KeepON is to have the NIC keep on transmitting fixed-size data chunks as placeholders, thereby maintaining a predictable temporal transmission pattern. The real-time packets generated by the mission-critical application(s) will then be precisely inserted into this stream by replacing placeholders at the designated position to ensure their accurate transmission time. We implement and evaluate KeepON by modifying the network driver on a Raspberry Pi using its standard NIC<sup>1</sup>. Our experiments demonstrate that KeepON can achieve  $\times 162$  times scheduling accuracy comparable to its default driver, and  $\times 2.6$  times compared to hardware-based solution, thus enabling precise timing control on standard commodity hardware. A case study in a TSN testbed confirms KeepON's ability to maintain nanosecond-scale timing accuracy across multiple hops and concurrent flows.

## 1 Introduction

Many networked industrial applications, such as closed-loop control, distributed monitoring, and time-critical actuation, rely on deterministic packet transmission to meet their stringent timing requirements [9, 25, 29, 43, 49, 51]. In such systems, the correctness of operation is dependent not only on functional data delivery but also on the timing guarantee that packets are delivered within bounded delay and jitter,

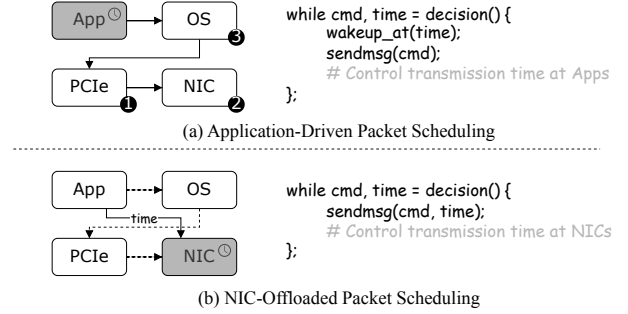


**Figure 1.** Comparison of packet transmission timing control methods on end devices.

summarized in Table 1. To meet such requirements, various deterministic networking technologies (e.g., Time-Sensitive Networking (TSN) and Deterministic Networking (DetNet)) have been developed to provide predictable data transport across the network [1, 15, 34, 50]. While these network infrastructures are often equipped with dedicated mechanisms to enforce timing guarantees within the network, the end devices at which packets originate or terminate are commonly built on general-purpose computing platforms [8, 31, 48, 52]. This disparity at the network endpoints undermines the end-to-end determinism that the network infrastructure alone cannot enforce, ultimately limiting the ability of the system to provide deterministic data delivery.

**Delay Components on End Devices.** When a real-time flow is transmitted over a deterministic network, the data originates from the application layer on the end device, typically through a system call (e.g., `send_msg`) that requests the operating system to dispatch the packet toward the network interface, as shown in Figure 1(a). The path of this data flow from the user space to the physical medium, however, includes a series of processing stages that collectively introduce non-deterministic delay. These delays originate from both operating system behavior and architectural constraints, and together they pose significant challenges to the deterministic timing performance of end systems.

**Table 1.** Summary of delay and jitter requirements for device capabilities in deterministic networks, as specified by industrial profiles [11, 17, 33].

Standard/Profile	Tx/Rx Delay	Tx/Rx Jitter
IEC/IEEE 60802	MAC delay $< 1\mu\text{s}$	MAC jitter $< 1\mu\text{s}$
IEEE P802.1 DP	E2E delay $< 10\mu\text{s}$	E2E jitter $< 1\mu\text{s}$
IIC Testbed	E2E delay $< 2\text{ms}$	E2E jitter $< 2\text{ms}$

<sup>1</sup><https://github.com/ChuanyuXue/KeepON-rpi>

- *Architecture-level delay*. One major source of timing variability stems from contention on the PCIe fabric (❶), where multiple concurrent data transfers can cause unpredictable access latencies in the order of 10  $\mu$ s [8, 31, 48]. Memory-mapped I/O (MMIO) operations (❶) may also experience fluctuating delays depending on the system load (e.g., worsened by small-write bursts) and cache coherency mechanisms [13, 40]. Other sources of architecture-level delay include batching mechanisms used by modern PCIe and NICs (❶, ❷), fetching policies implemented on NICs (❷), and latency introduced by I/O Memory Management Unit [1, 3, 6, 19, 32].
- *OS-level delay* (❸). Further sources of non-determinism emerge due to the general-purpose nature of modern kernels, even when enabled with real-time capabilities. For example, dynamic resource management mechanisms, e.g., dynamic socket buffer tuning, introduce delay variability from buffer reallocation or page fault under memory pressure [28]. In addition, interrupts, context switches and task preemption in the network stack and scheduling process can both result in unpredictable delays [44, 48].

To deal with these non-deterministic timing variability, an increasingly adopted approach is to offload the responsibility of precise packet timing control from the OS (e.g., real-time scheduling, interrupt management) to the NIC [6, 8, 19, 30, 48]. Examples include Intel’s LaunchTime feature on i210/i225 controllers, NVIDIA Mellanox’s Accurate Scheduling technology, and IEEE 802.1Qbv Time-Aware Shaper [1, 3, 32]. This approach fundamentally changes the timing control paradigm. As shown in Figure 1(b), rather than relying on the CPU to initiate transmission at a specific time, the driver specifies a future transmission timestamp, and the NIC independently takes responsibility to enforce it. Once the timestamp is set, the packet resides in the NIC’s hardware queue until the scheduled time when it is released onto the network medium. This strategy essentially bypasses all the previously discussed sources of non-deterministic delay.

Supporting such functionality requires the NIC to have two distinct hardware capabilities: 1) a local onboard hardware clock with high-precision synchronization (typically via IEEE 1588 PTP), and 2) specific logic to schedule packet transmissions according to timestamps using that clock. However, after surveying 341 drivers from Linux kernel 6.12, we identify that only 46 drivers (13.5%) support IEEE 1588 PTP hardware clock and only 13 drivers (3.8%) support hardware offloading for scheduled transmission (see Table 2). Thus, NICs with both required hardware support remain absent in most of the standard commodities. To address this, we propose a novel software-based driver model, namely KeepON, to support deterministic packet transmission on general-purpose end devices. Specifically, we make the following contributions:

- We design KeepON, a novel driver model that achieves deterministic packet transmission on standard commodity

NICs. KeepON leverages fundamental NIC operational characteristics in constant NIC transmission and error detection to provide determinism without requiring specialized hardware features.

- Building upon the KeepON driver model, we enable end-to-end determinism support for heterogeneous traffic transmission by the design and implementation of two modules: 1) network-wide clock synchronization and 2) heterogeneous traffic management.

- We prototype KeepON by modifying the existing Linux driver. Extensive experimental evaluation demonstrates that KeepON can achieve deterministic packet transmission and outperform software-based solution with the standard driver, and achieve comparable results to hardware-based solution, in terms of transmission jitter and synchronization accuracy.

## 2 Experimental Observations

To support the proposed software-based approach to enable deterministic transmission on commodity NICs, we conduct a set of experiments to examine the fundamental behaviors of typical NIC hardware. Our experimental setup consists of two machines directly connected via their Ethernet interfaces over a 1 Gbps link. On the sender machine, we vary the configurations, employing different commodity NICs and network utilization. The receiving machine is consistently equipped with an Intel i210 NIC, chosen for its reliable hardware timestamping for receiving packets. Please see §7 for more details of the experimental settings.

In the first set of experiments, we measure the transmission finish times of fixed-size Ethernet frames (1500 bytes) under various NIC and OS configurations, with the network utilization set to 50%, 80%, and 100% of the line rate. The results in Figure 2 reveal that when the NIC operates at 100% line rate, the transmission finish times exhibit a clear and consistent linear relationship with the packet index, with variation  $\sigma^2 \leq 16$  ns. In contrast, under lower levels of network utilization (e.g., 50% and 80%), the finish times show significant variations ( $\sigma^2 \approx 10^7$  ns), and the linearity with respect to the packet index is disrupted<sup>2</sup>. Based on these results, we have the following observation.

**Observation 1.** *A NIC can transmit fixed-size Ethernet frames at the physical line rate with deterministic timing performance.*

Observation 1 indicates that the time interval between successive transmissions becomes effectively constant if the NIC transmits fixed-size frames at the line rate, and the NIC’s progress through its transmission queue can be used as a proxy for elapsed time. This implies that by counting the number of packets transmitted, the system can reliably

<sup>2</sup>The observation is reproducible on all devices we have tested by simply running: `sudo iperf -u -c <address> -b 1000M`.

**Table 2.** 13 out of 341 Ethernet drivers in Linux 6.14 with hardware support for scheduled transmission offloading.

Driver	igb/igc	enetc	mlx4/5	bnxt	atlantic	cpsw	stmmac	rtsn	xilinx	engleder	lan966x
Vendor	Intel	NXP	Nvidia	Broadcom	Aquantia	TI	STMicro	Renesas	Nvidia	Engleder	Microchip
SO_TXTIME	✓	✓	✓	✓	✓	-	-	-	-	-	-
TAPRIO	✓	✓	-	-	-	✓	✓	✓	✓	✓	✓

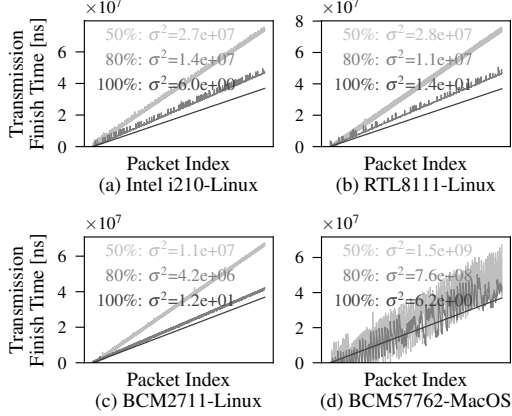


**Figure 2.** Packet transmission finish time for fixed-size Ethernet frames under varying network loads across 4 different NIC/OS configurations.

estimate the relative passage of time, assuming the NIC is occupied by back-to-back packet transmissions.

In the second set of experiments, we measure the CPU utilization associated with packet reception at the receiving machine while varying the ratio of corrupted packets, e.g., with bad Cyclic Redundancy Check (CRC) code, within a fixed batch of 32 packets. The experiments are performed under different Ethernet frame sizes, specifically 100 bytes and 1500 bytes. The results in Figure 3 demonstrate a clear trend: as the number of corrupted packets within each batch increases, the CPU utilization on the receiving machine decreases significantly. For instance, with 100-byte frames, CPU utilization drops sharply from nearly 100% when no packets are corrupted to almost 0% when all 32 packets in the batch are corrupted. A similar trend is observed for 1500-byte packets, where CPU utilization decreases from 6.9% to just 0.3%

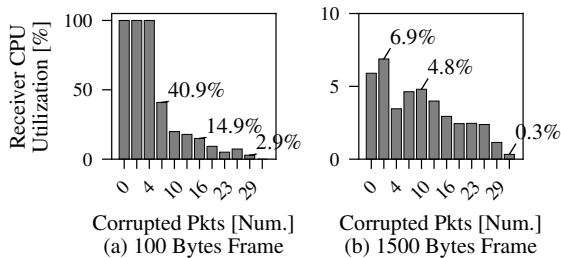


**Figure 3.** The CPU utilization at the receiving machine when processing a line-rate stream composed of repeating 32-packet batches.

as the number of corrupted packets increases from zero to 32. These results indicate that the reception of corrupted packets imposes minimal processing overhead on the CPU. Based on these experimental results, we conclude:

**Observation 2.** *Commodity NICs include built-in error detection logic that detects and discards corrupted packets before the packet reaches the host memory at the receiver.*

Observation 2 stems from the standard operation of Ethernet networks and the NIC design, where such capability is typically implemented directly in hardware and is part of the Ethernet protocol stack [22]. As a result, the receiver NIC can efficiently distinguish between valid and invalid packets through hardware CRC checking without introducing additional CPU overhead, as shown in the experiments. Performing such checks and discard operations directly in hardware enables the system to inject a controlled stream of "fake" packets with the assurance that they will be dropped by the receiver without introducing any host CPU overhead. This capability has been previously noted in the MoonGen project for generating high-rate network traffic with arbitrary patterns [12].

### 3 System Design

The two observations discussed above reveal important behaviors of commodity NICs that can be leveraged to achieve precise timing control without requiring specialized hardware support. Specifically, *Observation 1* provides a NIC-level clock by counting the number of transmitted packets when the NIC continuously transmits fixed-size packets at line rate. *Observation 2* provides the essential mechanism to sustain continuous transmission at the line rate through injecting intentionally corrupted packets into the transmission stream, even when the application data is sparse. Together, these observations provide the foundation for a software-controlled mechanism that emulates deterministic transmission timing using standard NIC hardware by carefully controlling both the rate and composition of outgoing packet streams.

In this section, we discuss the architecture of our proposed driver model, KeepON, as shown in Figure 4. At the highest level, KeepON aims to meet three goals.

- **G1: Hardware independency:** Operating on standard NICs without requiring specialized hardware features.
- **G2: Deterministic real-time communication:** Guaranteeing bounded latency with minimal jitter for end-to-end packet transmissions.

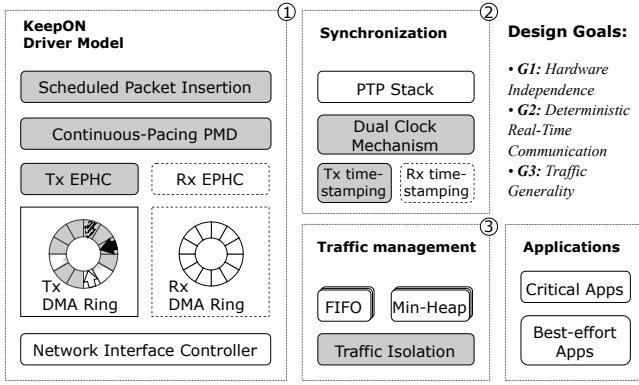


**Figure 4.** The high-level architecture of KeepON with the grey blocks highlighting our design components. Dashed-line blocks represent optional components for performance tuning (e.g., Rx-EPHC and Rx timestamping).

• **G3: Traffic Generality:** Supporting heterogeneous traffic types, including both real-time flows and best-effort flows.

To achieve these goals, the KeepON driver model (①) is in place to provide the basic functionalities and it comprises three components: 1) Continuous-Pacing Poll Mode Driver (CP-PMD) to maintain a continuous stream of packet transmission at line rate; 2) Emulated PTP Hardware Clock (EPHC) to provide clock function; 3) Scheduled Packet Insertion to precisely and efficiently insert application packets into the continuous stream. Building upon these fundamental capabilities for precise timing control at the end device, we further propose a *Synchronization* (②) module to synchronize the EPHC across multiple devices, thus being able to enable end-to-end deterministic real-time communication.

Since industrial applications often involve a combination of critical real-time traffic and non-critical best-effort traffic, we further propose a *Traffic Management* (③) module to support heterogeneous traffic types. This module performs traffic isolation via DMA ring partitioning and traffic pre-buffering using dedicated queues to ensure determinism of real-time applications.

By integrating the above modules, KeepON provides a comprehensive solution to achieve end-to-end deterministic real-time communication on commodity hardware while also supporting the co-existence of heterogeneous traffic.

## 4 KeepON Driver Model

This section describes the component design of KeepON.

### 4.1 Continuous-Pacing PMD (CP-PMD)

Instead of transmitting packets on demand as performed by conventional drivers, the key functionality of CP-PMD is to enable constant NIC transmission by filling idle bandwidth with corrupted packets. To achieve this, CP-PMD operates on the pre-initialized ring buffer filled with descriptors of fixed-size and corrupted packets.

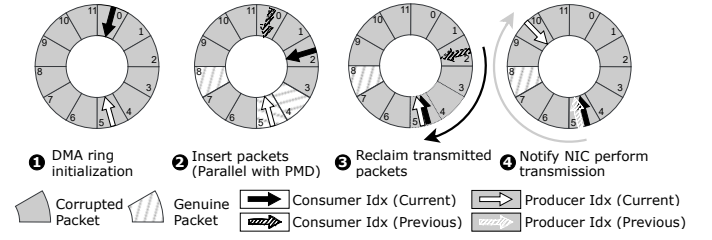


**Figure 5.** DMA ring management operations in the KeepON driver model, illustrating both the Continuous-Pacing PMD (§4.1) and Scheduled Packet Insertion (§4.3).

Figure 5 shows an example of a DMA ring buffer with 12 descriptors (①). It implements a persistent polling loop in three steps: 1) Identify Transmitted Packets: The driver queries the current consumer index, identifying descriptors whose transmission has been completed. For example, the consumer index (black arrow) moves from 2 to 5, signifying that 3, 4, and 5 are transmitted (②); 2) Reclaim and Reset Descriptors: It resets the completed descriptors (4, 5) back to the placeholder state with corrupted-CRC (③), marking them as available for subsequent overwrites by the packet insertion mechanism (to be discussed in §4.3); 3) Advance Producer Index: PMD consistently advances the producer index by a certain batch size, informing the NIC how far it should continue to process descriptors in the ring buffer (④). This continuous cycle of querying, resetting, and advancing indices ensures that the NIC hardware maintains continuous line-rate operation, regardless of whether any new application packets are inserted into the ring.

**Parameter Settings.** In CP-PMD, the setting of two parameters, i.e., slot size and batch size, can affect the system performance, e.g., real-time performance, CPU usage, and clock accuracy. The slot size determines the time granularity of packet transmissions. A smaller slot size enables finer-grained control over transmission timing but may increase system overhead due to more frequent packet handling. The batch size specifies the number of descriptors that the producer index advances in each polling iteration (e.g., batch size is 5 in Fig. 5 (④)). A larger batch size reduces per-packet processing costs, thus lowering CPU and PCIe overheads. But it comes at the expense of reduced timing granularity, lower clock accuracy, and the flexibility in packet scheduling (immediate insertion window in §4.3).

**Experimental Validation.** We evaluate the effectiveness of the KeepON driver model in achieving deterministic packet transmission by measuring the packet inter-arrival jitter at the receiver. We vary the transmission period from 200  $\mu$ s to 1000  $\mu$ s and compare KeepON with the conventional driver (GENET) as the baseline and a driver (IGB) where its NIC (Intel i210) supports hardware scheduling offloading. We set the slot size and batch size to 1230 bytes and 1, respectively. As shown in Figure 6, KeepON significantly outperforms the

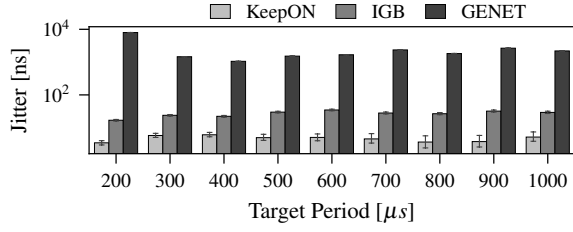


**Figure 6.** Packet inter-arrival jitter comparison among KeepON, conventional driver, and hardware offloading approach under varying period settings. The error bars represent standard deviations.

baseline, with 99.9% of the measured jitter values falling below 16 ns, whereas the GENET exhibits jitter on the order of several thousand nanoseconds. Most importantly, KeepON also surpasses the hardware-supported approach IGB, achieving an average jitter approximately four times lower than that provided by hardware offloading. This is because the Intel i210 NIC’s scheduling function has a resolution of 32 ns, described in its technical datasheet [23].

#### 4.2 Emulated PTP Hardware Clock

Enabling applications to schedule transmissions at precise timestamps on the NIC requires mapping the desired time instant to a specific DMA ring slot. To achieve this, we introduce the Emulated PTP Hardware Clock (EPHC) to provide a clock domain derived from the NIC’s packet counter.

**Clock Specification.** EPHC maps the constant-rate physical layer activity, enforced by CP-PMD, to a time base. To realize the mapping, we employ a linear clock model comprising three key components, where the current time is calculated as:  $\text{cycle-count} \times \text{cycle-period} + \text{offset}$ .

- *Cycle-count* is derived by the packet counter, which increments with each transmitted packet and serves as the “ticks” of the emulated clock.
- *Cycle-period* defines the duration of each transmission cycle and equals the division of slot size by line rate.
- *Offset* serves as the clock’s epoch, aligning the origin of the emulated clock to a meaningful global time reference, such as UTC time [2]. It is obtained in the initialization phase.

**Clock Accuracy Measurements.** We compare the clock quality of the proposed EPHC with the Intel i210 NIC’s hardware PTP clock (PHC). To assess accuracy, each clock is used to toggle a GPIO pin, generating a square wave with a target period of  $36 \mu\text{s}$ <sup>3</sup>. As shown in Figure 7, the EPHC achieves a

<sup>3</sup>The actual periods of the resulting GPIO-generated square wave, which directly reflect the precision of the controlling clock, are measured using a Tektronix TBS2000B 200 MHz oscilloscope. This indirect method of using the clock to create a measurable physical signal is employed because the software-emulated EPHC’s timing data cannot be directly interfaced with an oscilloscope. We set a  $36 \mu\text{s}$  target wave because it is a multiple of EPHC’s clock granularity when we set the slot size to 1500 bytes.

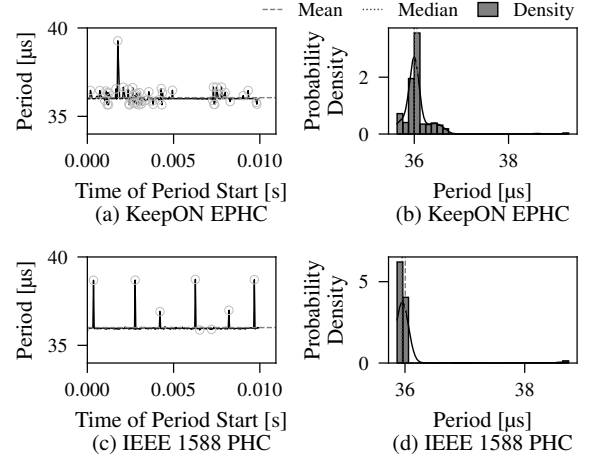


**Figure 7.** Comparison of clock accuracy of KeepON’s EPHC (Fig.(a)&(b)) and IEEE 1588 hardware clock (Fig.(c)&(d)), both targeting a  $36 \mu\text{s}$  period.

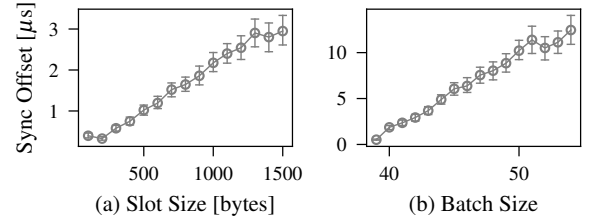


**Figure 8.** Impact of slot size and batch size on the EPHC clock stability, evaluated by measuring the absolute time offset between the EPHC clock and system UTC clock.

mean and median period closely matching the target, demonstrating comparable central tendency to the hardware clock. However, EPHC exhibits higher jitter, reflected in the wider distribution of its measured periods in Figure 7(b) compared to the tighter distribution for the PHC in Figure 7(d). This increased jitter primarily stems from the granularity limits of EPHC’s packet-counting-based time estimation. Nevertheless, most of EPHC’s jitter remains within  $\leq 1 \mu\text{s}$  of the mean, indicating relatively controlled variation.

We further investigate how the slot size and batch size settings affect the clock stability of EPHC by continuously measuring the absolute offset between the EPHC and the system UTC clock. Figure 8 shows that both a larger slot size and a larger batch size lead to larger clock offsets. The former is due to the larger clock granularity and the latter is caused by the less frequent clock update. In the experiments, we also notice that the offset is negligible ( $\leq 1 \mu\text{s}$ ) when the batch size is set smaller than 39.

**Clock Adjustment:** Since the EPHC clock needs to synchronize with other clocks in the network, two types of clock adjustments are supported. 1) *Offset Adjustment* aligns the EPHC’s time reference by either applying a fixed offset correction or directly setting the clock to a specified time.

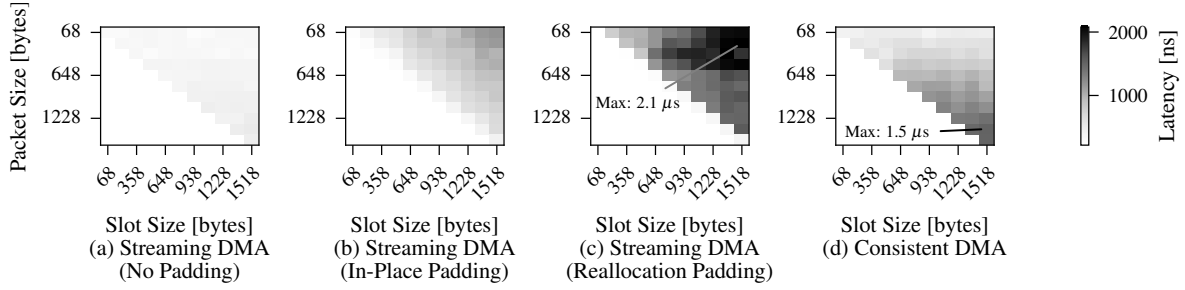


**Figure 9.** Latency comparison for different padding strategies. Heatmaps show latency for padding (lighter is lower/better) based on packet size (y-axis) vs. target DMA slot size (x-axis).

2) *Rate adjustment* modifies the cycle-period, effectively adjusting the emulated clock’s progression rate to correct for frequency drift and maintain long-term alignment with a reference clock. These clock adjustments never modify the cycle count, which remains a monotonic counter tied solely to packet transmissions. This design principle ensures that transmission scheduling remains undisrupted during clock synchronization.

### 4.3 Scheduled Packet Insertion

Unlike traditional drivers, which process packet descriptors in an FIFO manner, KeepON performs scheduled packet insertion and overwrites placeholder descriptors at specific indices in the DMA ring to achieve scheduled transmissions.

**Insertion Process.** When an outgoing packet arrives at the driver with its designated scheduled time in the EPHC clock domain, the driver calculates the target slot in the DMA ring and performs three validation checks. 1) It verifies that the target slot is occupied by a placeholder descriptor associated with a corrupted CRC. 2) The target slot must be sufficiently ahead of the NIC’s current consumer index by at least one batch size, and before the consumer index wraps around in the next cycle to maintain a safe temporal margin, i.e., within immediate insertion window [ $c\_index + \text{batch size}$ ,  $c\_index + \text{ring size}$ ). 3) It verifies that the incoming packet’s application has ownership of the target slot (more details are discussed in §6.1). If all the validation checks succeed, the driver pads the packet to match the slot size and inserts it into the ring buffer at the target slot index. For example, as shown in Figure 5, packets are inserted at slots 4, 5, and 8 (2), rather than being appended sequentially to the queue as in a conventional driver. After insertion, the driver updates the corresponding descriptor to mark the slot as valid by setting the CRC field to a correct value. If any validation check fails, the driver discards the packet and returns an error code to the application.

One challenge in packet insertion is padding outgoing packets to match fixed-size slots, which introduces significant memory write delays. Traditional drivers use zero-copy transmission with standard streaming DMA, directly mapping packet buffers (skbs) to the NIC’s DMA engine and unmapping them after transmission. This incurs a small and

size-independent per-packet map/unmap overhead ( $\leq 0.5 \mu\text{s}$ ), as shown in Figure 9(a). However, zero-copy transmission loses its performance advantage when packets require padding, where the driver must write zeros to fill empty slot space, creating significant overhead for small packets in large slots, as shown in Figure 9(b). Even worse, if the skb lacks sufficient tailroom, a costly re-allocation, copy, padding (memset), and remapping sequence is triggered, adding significant and unpredictable latency. Figure 9(c) shows that this reallocation path often incurs latency exceeding  $2 \mu\text{s}$ . Tests on Linux kernel 6.12 with uniformly distributed packet sizes reveal how frequently this occurs: for UDP and raw sockets, 37.5% of packets lack sufficient skb tailroom for slot padding, and for TCP, tailroom is always zero. This confirms that relying on streaming DMA for padding frequently triggers the costly reallocation behavior.

**Packet Padding.** To address the padding overhead, we propose to use consistent DMA by pre-allocating and permanently mapping fixed-size buffers that match the transmission slot size. When a new packet arrives, its payload is copied directly into the designated pre-mapped buffer, trading map/unmap overhead for a predictable memory copy cost. As shown in Figure 9(d), this approach keeps the packet insertion latency within  $1.5 \mu\text{s}$ , primarily determined by the payload size. More importantly, since the buffers are fixed-size and reused, padding (zeroing the unused portion) can be efficiently deferred to CP-PMD’s polling phase (4 in Figure 5) when resetting descriptors. This shifts the memory write overhead off the critical packet insertion path, leaving only the payload memcpy cost during scheduling.

We compare the total latency in the driver’s transmit path, measured from the moment when a packet arrives at the driver to the time when it is handed over to the NIC. Figure 10(a) shows the median delay of the KeepON driver and GENET. KeepON consistently achieves lower latency, with an average delay of  $7 \mu\text{s}$  compared to  $11 \mu\text{s}$  for the baseline. This improvement primarily results from eliminating the DMA mapping/unmapping overhead and avoiding the IOMMU doorbell operation typically required to notify the NIC for transmission. By moving NIC notifications out of the critical data path (handled by the PMD), KeepON reduces transmission overhead and latency. Figure 10(b) compares the

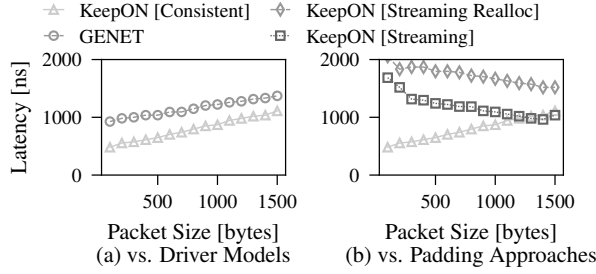


**Figure 10.** Comparison of total driver transmit path latency. (a) Median delay of KeepON and GENET. (b) Median delay of different padding approaches, comparing streaming DMA (w/o sufficient tailroom) versus consistent DMA.

impact of different padding strategies. When using streaming DMA (square-mark line), its performance is close to that of consistent DMA, when all incoming packets have sufficient tailroom for padding and large packets are handled ( $\geq 1200$  bytes). However, when tailroom is insufficient and reallocation is required, streaming DMA incurs significantly higher latency (diamond-mark line) due to padding, with an average delay of  $17 \mu\text{s}$ , compared to the consistent DMA.

## 5 Network-Wide Synchronization

To achieve end-to-end deterministic packet transmission, the EPHC clock must synchronize across other nodes to realize network-wide synchronization.

### 5.1 PTP Synchronization

We propose to synchronize the EPHC clock using the IEEE 1588 PTP [21], which corrects both time offset and frequency drift relative to a master clock. As illustrated in Figure 11, PTP operates via a timed message exchange requiring four timestamps: sync sent by master at  $t_1$ , sync received by slave at  $t_2$ , delay\_req sent by slave at  $t_3$ , and delay\_req received by master at  $t_4$ . Assuming symmetric network delay [21], the slave estimates the time offset each round of message exchange (①) as  $[(t_2 - t_1) - (t_4 - t_3)]/2$ , which is used to adjust the EPHC's *Offset*. Frequency differences, estimated by observing the change in offset over time, e.g., using two successive sync message timestamps  $t_1/t_2$  and  $t_1^{next}/t_2^{next}$ , are used to adjust the EPHC's rate parameter (②).

Obtaining precise timestamps ( $t_1, t_2, t_3, t_4$ ) within a driver or OS is challenging due to the inherent and random transmit delay and receive delay, i.e.,  $J^{out}$  and  $J^{in}$  in Figure 11, respectively. Since KeepON enables the deterministic packet scheduling function, we are able to mitigate the uncertainty in Tx timestamping by calculating the outgoing EPHC time. For receive timestamps, we follow the software timestamping approach where receive delays are inevitable.

**Synchronization Accuracy Measurements.** We compare the PTP synchronization accuracy among KeepON, GENET, and IGB in a single-hop network with slot size and batch

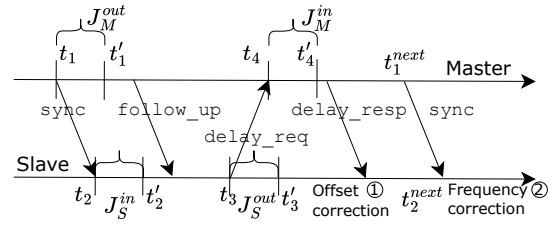


**Figure 11.** Single-hop packet exchange and timestamping for PTP synchronization between master and slave demonstrating the calculation of clock offset and frequency adjustments.

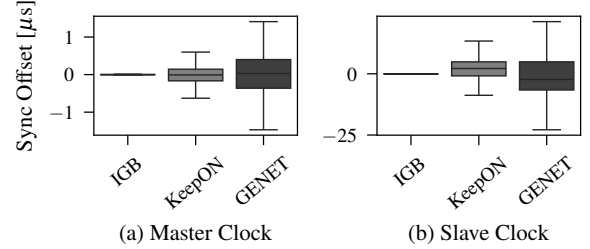


**Figure 12.** PTP synchronization accuracy comparison among KeepON, GENET, and IGB in a single-hop network.

size in DMA set to 300 bytes and 1, respectively. As shown in Figure 12, hardware timestamping achieves the highest accuracy as expected (around  $0.015 \mu\text{s}$  as both master and slave). On the other hand, KeepON demonstrates significantly improved synchronization accuracy ( $0.3 \mu\text{s}$  as master and  $3.7 \mu\text{s}$  as slave) over software timestamping ( $0.5 \mu\text{s}$  as master and  $6.9 \mu\text{s}$  as slave), due to more precise Tx timestamps. To better understand the synchronization offset that arises from inaccurate Tx/Rx timestamping, we also conduct a theoretical synchronization analysis, which is provided in Appendix §A.5.

### 5.2 Dual Clock Mechanism

To address the inherent inaccuracy of receive timestamps, we introduce an optional Dual Clock Mechanism that maintains two distinct EPHC clocks simultaneously. We establish a second Rx-EPHC, driven by a packet counter tracking incoming packets on the receive path. This requires the remote peer device also to transmit packets continuously at the line rate, to ensure a stable stream of incoming packets to drive the Rx counter. The receive path utilizes another CP-PMD polling loop dedicated to monitoring the Rx DMA ring.

**Clock Merging.** The proposed dual EPHC setup provides two independent clocks and more accurate timestamping mechanism for both transmit and receive paths. However, the system requires a unified time reference for overall consistent operation and PTP synchronization. Therefore, we propose a clock merging algorithm to derive a unified clock time by dynamically merging the instantaneous values from the Tx-EPHC  $T_{tx}$  and Rx-EPHC  $T_{rx}$ . The algorithm handles two cases:



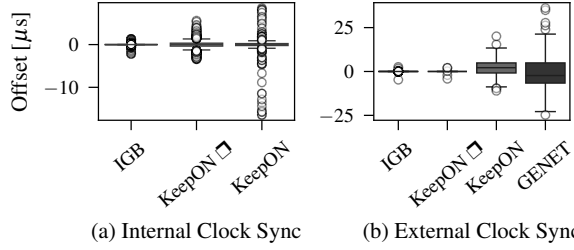


**Figure 13.** Comparison of clock quality and synchronization accuracy for single clock (KeepON), dual clock (KeepON □), software clock (GENET) and hardware clock (IGB).

- *Large divergence:* If the absolute difference  $|T_{tx} - T_{rx}|$  exceeds a predefined  $2\tau$  worst-case clock jitter, we set the lagging clock to the leading clock. This is based on our practical observation of PMD that if the two clocks diverge significantly, it indicates a potential fault in the slower clock due to traffic burst or system jitter.

- *Small divergence:* If the clocks are consistent with  $|T_{tx} - T_{rx}| \leq 2\tau$ , their values are combined using a heuristic function to produce a merged timestamp. Under a non-faulty state, we observe that clock jitter is predominantly due to delayed clock updates. Thus, we implement the merging function as  $[\max(T_{tx}, T_{rx}) + \min(T_{tx} + \tau, T_{rx} + \tau)]/2$ . Then, assuming  $T_{tx}$  and  $T_{rx}$  have equal clock performance, the maximum possible jitter of the merged timestamp is reduced from  $\tau$  to  $\tau/2$ .

**Experimental Validation.** Our experimental results show that the dual clock mechanism not only significantly improves synchronization accuracy but also improves clock quality. Figure 13(a) compares the clock quality, where the dual clock mechanism (KeepON □) achieves slightly better stability with an absolute offset of  $0.58 \mu s$ , compared to the single clock mechanism (KeepON) with an absolute offset of  $0.64 \mu s$ . More importantly, KeepON □ has a much better 99th value of  $5.3 \mu s$ , compared to that of KeepON ( $16.4 \mu s$ ). This is because KeepON □ tends to merge two clocks with a large divergence to correct potential faults. Figure 13(b) shows the synchronization accuracy by comparing the offset with external clock. KeepON □ achieves significantly better accuracy with an absolute offset of 10 ns, compared to KeepON with  $3.8 \mu s$ . Moreover, KeepON □ is shown to be slightly better than the hardware clock with an average absolute offset of 15 ns.

## 6 Heterogeneous Traffic Management

Industrial applications often involve heterogeneous traffic with diverse characteristics and service requirements, e.g., real-time URLLC traffic and best-effort eMBB traffic in 5G industrial networks [42]. To enable KeepON to handle heterogeneous traffic, in this section, we introduce the traffic isolation module which partitions the DMA ring buffer to isolate different types of traffic from interference.

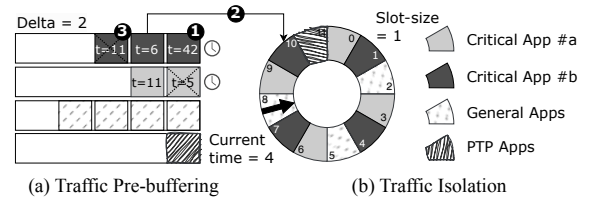


**Figure 14.** An illustration of traffic pre-buffering and traffic isolation mechanisms, including partitions for two real-time traffic classes (critical App#a and App#b), and two best-efforts traffic classes (general services and PTP).

### 6.1 Traffic Isolation

To achieve traffic isolation, we partition the DMA ring buffer into dedicated regions. For example, as shown in Figure 14(b), the DMA ring buffer is partitioned into four distinct regions, each of which is assigned to an individual traffic class. Typically, each traffic class is assigned to a dedicated critical application, e.g., App #a and App #b, but it can also serve one or multiple best-effort applications. If the packet of an application intends to be inserted into a slot in the ring buffer that is reserved for another traffic class (e.g., App #a inserts  $t=11$ , belongs to App #b ②), the packet will be dropped.

Based on the partitioning mechanism, we need to determine the partition allocated to each traffic class to ensure that the resources specified by the partition can meet the timing requirements of the critical application. To achieve this, we model this as a resource partitioning and traffic scheduling problem and provide the definition of a feasible schedule guaranteeing their timing requirements.

**Traffic Scheduling Model.** 1) *DMA Ring Buffer:* A ring buffer  $B$  is equally divided into  $N$  descriptor slots  $s \in \{0, 1, \dots, N-1\}$ . The transmission time of each slot is constant as  $\delta$  (depending on the slot size), and slot  $s$  is available for a transmission to start at  $t$ , when  $s \equiv \lfloor t/\delta \rfloor \bmod N$ . We assume each slot only handles one packet transmission.

2) *Critical Apps:* A critical application set  $\mathcal{A} = \{A_1, A_2, \dots, A_K\}$  share the single buffer with best-effort applications. Each critical application  $A_i$  runs a set of real-time flows. Each flow  $j \in A_i$  is characterized by its packet release period  $p_{i,j}$  and maximum allowed jitter  $j_{i,j}$  relative to the release period. Assume  $p_{i,j}$  is multiples of  $\delta$ . The hyperperiod  $H$  is the least common multiple of all the flow periods in all the critical applications, i.e.,  $H = LCM(\{p_{i,j} \mid A_i \in \mathcal{A}, j \in A_i\})$ .

3) *Partitions:* A partition set  $\mathcal{F} = \{f_1, f_2, \dots, f_K\}$  consists of disjoint partitions each of which corresponds to a subset of slots in the ring buffer, i.e.,  $f_i \subseteq B$ , and is allocated to  $A_i$ .

**Per-Application Schedule Definition.** A schedule  $S_i$  is defined for each application  $A_i$  specifying the transmission time for all its flows in the hyperperiod using the slots in partition  $f_i$ . Each flow  $j$  releases  $M_j = H/p_{i,j}$  instances in the hyperperiod, and the transmission time for any instance, denoted as



$t_{i,j,l}$ , is determined by schedule  $\mathcal{S}_i$ . Correspondingly, the slot used for transmitting the instance is  $s_{i,j,l} = \lfloor t_{i,j,l} / \delta \rfloor \bmod N$ .

**Valid Schedule.** A schedule  $\mathcal{S}_i$  generated for application  $A_i$  using the allocated partition  $f_i$  is valid if  $\mathcal{S}_i$  satisfies the following constraints for all flows  $j \in A_i$ :

1) The slot used for transmitting each instance of application  $A_i$ 's flows must be within the partition allocated to  $A_i$ , i.e.,

$$\forall i, j, l, s_{i,j,l} = \lfloor t_{i,j,l} / \delta \rfloor \bmod N \in f_i. \quad (1)$$

2) The time difference between any two packet transmissions ( $|t_{i,j,a} - t_{i,j,b}|$ ) must not deviate from the difference in their specified release times ( $|(a - b)| \cdot p_{i,j}$ ) by more than the jitter  $j_{i,j}$ , i.e.,

$$\forall i, j, a \neq b, ||(t_{i,j,a} - t_{i,j,b})| - |(a - b)| \cdot p_{i,j}| \leq j_{i,j}. \quad (2)$$

3) Any two packets within the same application cannot transmit at the same time, i.e.,  $\forall i, j \neq j', l \neq l', t_{i,j,l} \neq t_{i,j',l'}$ .

The partitioning problem is to find a feasible partition set  $\mathcal{F}$  such that at least one valid schedule  $\mathcal{S}_i$  exists for each  $A_i$  using partition  $f_i$ . To determine a valid set of partitions  $\mathcal{F}$  and schedules  $\mathcal{S}_i$  for all critical applications, we can employ Satisfiability Modulo Theories (SMT) [5] to translate the above variables and constraints into a system of logical and arithmetic constraints. An SMT solver, such as Z3 [10], can systematically search for a solution that satisfies all these constraints. If a solution is found, it readily provides a feasible partition and schedule; conversely, if the solver returns unsatisfiability, it indicates that no available partition exists under the given parameters. In this case, one can either increase the DMA ring size or change the efficiency parameters of PMD, e.g., reducing the slot size.

## 6.2 Traffic Pre-Buffering

If applications submit packets too early before the scheduled times that fall out of the range of the immediate insertion window discussed in §4.3, the packets need to be pre-buffered until the available window. To address this, we introduce the *traffic pre-buffering* mechanism. This involves maintaining intermediate software queues that decouple packet submission from immediate DMA insertion, allowing for orderly management and timely hand-off based on traffic class. Figure 14(a) illustrates this concept, where packets are pre-buffered in software queues before being inserted into the DMA ring buffer.

- *Real-time traffic:* Real-time traffic packets, with application-defined target transmission times, are managed in a min-heap pre-buffering queue ordered by their scheduled timestamps [39]. A separate software component periodically checks the heap's root packet (earliest schedule) against the EPHC's current time. If the root packet's scheduled time enters immediate insertion window, it's removed from the heap and sent to the PMD for scheduled insertion. The min-heap ensures real-time packets are inserted in earliest deadline first order.

- *Best-effort traffic:* Best-effort traffic, lacking precise deadlines, uses a simpler FIFO queue for pre-buffering, with packets enqueued as received. When the Traffic Isolation logic identifies an available slot in the designated DMA ring partition (e.g., a placeholder slot at near future), a packet is dequeued from the FIFO's head. This packet is then sent to PMD to be placed into the next available placeholder slot within its assigned partition.

## 7 Evaluation

In this section, we evaluate the performance of KeepON on end devices, in terms of real-time performance, background traffic throughput, CPU utilization, and energy/thermal efficiency by comparing it with the default driver and hardware-based offloading solutions. We implement the KeepON driver model based on the GENET driver for the BCM2711 SoC's integrated Ethernet controller. Due to the page limit, the detailed implementation is provided in the Appendix §A.2.

### 7.1 Experiment Setup

In our experiments, we use a pair of end devices directly connected by an Ethernet cable back-to-back. Experiments run on a Raspberry Pi 4 Model B (Cortex-A72 @ 1.5GHz, 8GB LPDDR4 RAM) using the default onboard Ethernet adapter. We use its original driver (GENET) in Linux kernel version 6.12 for comparison to the proposed KeepON driver. To compare with hardware-based offloading solutions (IGB), we use the Intel i210 Ethernet controller with its default *igb* driver in Linux kernel version 6.12, and use a Raspberry Pi CM4 with PCIe I/O board with the same settings to support this external PCIe NIC. We configure Linux ETF Qdisc for each method, where KeepON uses it solely for pre-buffering; IGB uses it for pre-buffering with hardware offload enabled (leveraging the i210 NIC's scheduling capabilities); and GENET relies on ETF for software-based timing control. All experiments used a 1 Gbps line rate.

### 7.2 Deterministic Packet Transmission

We evaluate the real-time performance of KeepON in supporting deterministic packet transmission using two metrics: Packet Delay Variation (PDV) and inter-arrival jitter. PDV measures the variation in one-way latency experienced by real-time traffic, which reflects the transmission's timing accuracy but impacted by synchronization performance. Inter-arrival jitter characterizes the variability in packet transmission timing at the sender side over a back-to-back Ethernet connection, impacted by the sender's processing capability.

We compare KeepON with GENET and IGB under two background traffic load conditions, idle and busy, by varying the packet size of real-time traffic. The three approaches are deployed at the sender, and we use a NIC with IEEE 1588 PTP hardware stamping as the receiver for accurate measurement. Two devices are synchronized by the PTP

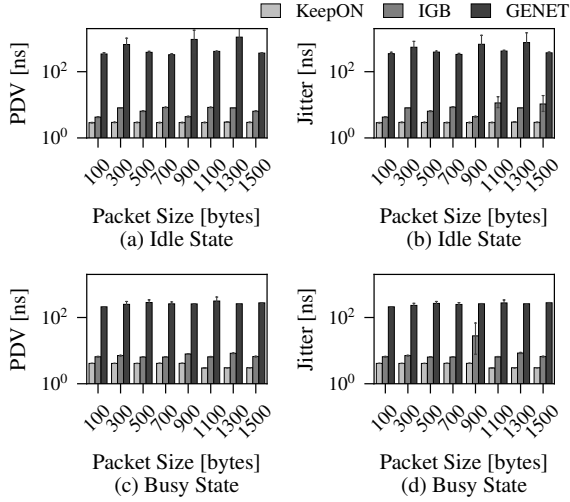


**Figure 15.** Deterministic performance comparisons in PDV and inter-arrival jitter among KeepON, GENET, and IGB under varying packet size settings.

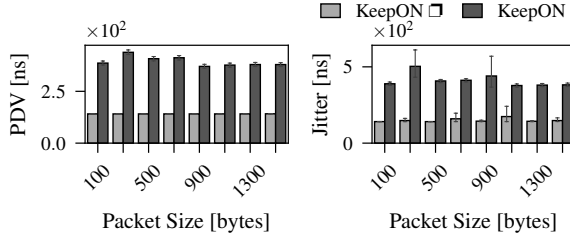


**Figure 16.** Deterministic performance comparisons of KeepON under single clock (KeepON) and dual clock (KeepON □) modes, measured by software timestamping.

protocol. For a busy state, we allocate sufficient slots for real-time traffic and PTP traffic. Then, use `ping -f -l 65535` to generate a large traffic to occupy background bandwidth. Each experiment transmits  $1 \times 10^6$  packets, and the error bar shows the standard deviation.

**Single Clock.** Under an idle background traffic load, as shown in Figure 15(a)&(b), KeepON achieves the lowest PDV of 2.9 ns, outperforming IGB (6.8 ns) and GENET (566.9 ns). KeepON also demonstrates superior inter-arrival jitter performance, recording 3.7 ns compared to 7.7 ns for IGB and 480.1 ns for GENET. Similar trends are observed under a busy background traffic load as shown in Figure 15(c)&(d), confirming that KeepON consistently delivers the best deterministic performance across varying network conditions. Interestingly, we also observe that the inter-arrival jitter of the hardware offloading solution is sometimes worse in PDV, e.g., at packet sizes of 1100 and 1500 bytes in the idle state, and 900 bytes in the busy state. We attribute this to additional delays introduced by the hardware offloading mechanism, which slows down packet transmissions and causes jitter accumulation. In contrast, KeepON maintains tight control

over transmission timing, avoiding such accumulative effects.

**Dual Clock.** Figure 16 shows the deterministic performance comparison of single clock (KeepON) and dual clock (KeepON □) modes by varying packet size<sup>4</sup>. The results show that the KeepON □ further improves determinism, achieving consistently low PDV and inter-arrival jitter, averaging 141 ns and 150 ns, respectively, compared to 381 ns and 416 ns in the single-clock mode. These results clearly demonstrate that clock synchronization between KeepON-enabled devices in dual-clock mode substantially enhances deterministic network performance.

### 7.3 Best-Effort Traffic Throughput

**Traffic Isolation.** In this set of experiments, we evaluate the effectiveness of the proposed traffic isolation mechanism on the DMA ring buffer by measuring the best-effort traffic throughput under different settings of slot allocation. We conduct bandwidth tests using `iPerf2` and vary the percentage of slot reservation for best-effort traffic. Specifically, KeepON-25%, KeepON-50%, and KeepON-100% reserve 8/32, 16/32, and 32/32 slots for best-effort traffic, respectively. The slots are allocated in a uniform manner and UDP packets with payloads of 200, 400, 600, and 1400 bytes are used. We run each test for 60 seconds and repeat the test 10 times to report the average.

As shown in Figure 17, KeepON can effectively regulate best-effort traffic throughput through traffic isolation, achieving predictable control over bandwidth allocation. Specifically, KeepON-100% delivers BE throughput comparable to that of the original driver (GENET) across various packet sizes and bandwidth settings. With 1400-byte packets, both the GENET and KeepON-100% approach the target bandwidth up to approximately 800 Mbps, after which saturation occurs. For smaller packets (e.g., 200 bytes), both methods exhibit lower saturation points due to the higher per-packet processing overhead on a single CPU core. Notably, KeepON-100% sometimes slightly outperforms the GENET under higher offered loads (e.g., above 600 Mbps), benefiting from PMD’s processing speed compared to interrupt-based. Under the KeepON-50% and KeepON-25% settings, the achievable BE throughput is limited to approximately 50% and 25% of the link capacity, respectively. These results confirm that KeepON accurately enforces bandwidth isolation through its ring isolation mechanism, ensuring that BE traffic does not interfere with reserved resources for real-time traffic.

**Packet Padding.** Figure 18 evaluates the overhead introduced by packet padding when the packet payload is smaller

<sup>4</sup>KeepON’s dual-clock mode requires both devices to operate with the KeepON driver model. This means that hardware timestamping, which is used for PDV comparisons in the single-clock mode (Figure 15), cannot be applied here and other solutions are not included (e.g., GENET and IGB); thus, software timestamping is used in Figure 16 for consistent comparison between KeepON’s two modes.

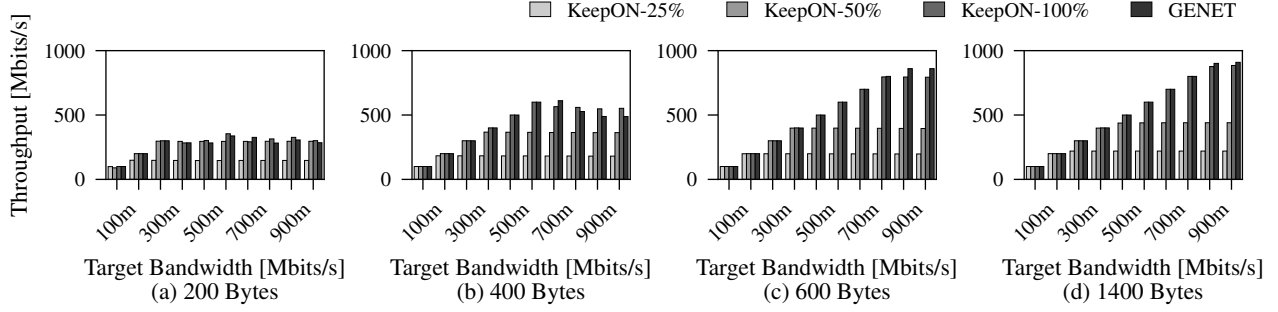


**Figure 17.** Best-effort traffic throughput under KeepON's traffic isolation mechanism with varying UDP packet sizes.

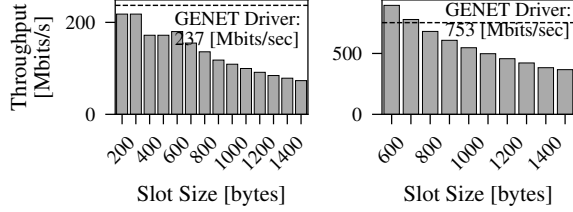


**Figure 18.** Evaluation of KeepON's fixed slot size mechanism and the impact of padding on UDP throughput.

than the slot size configured by KeepON. We send UDP traffic with fixed payloads of 100 bytes and 500 bytes under varying slot sizes. With a 100-byte payload (Figure 18(a)), maximum throughput of approximately 218 Mbps is achieved when the slot size is set to 200 or 300 bytes. As the slot size increases, throughput progressively declines, dropping to just 73.3 Mbps with a 1500-byte slot size. This demonstrates the impact of excessive padding, where transmitting 1400 bytes of padding for each 100-byte payload leads to bandwidth inefficiency. A similar pattern is observed with a 500-byte payload (Figure 18(b)) where the highest throughput of 895 Mbps occurs when using the smallest slot size that can accommodate the payload (600 bytes). As the slot size increases, throughput decreases accordingly, falling to 367 Mbps with a 1500-byte slot size. These results emphasize that selecting a slot size aligned with typical payload sizes is critical to reducing padding overhead and achieving efficient bandwidth utilization.

#### 7.4 CPU Utilization

The PMD operation of KeepON consumes CPU resources since it involves periodically reclaiming transmitted packet buffers and enabling continuous transmission at line-rate. Figure 19 evaluates the CPU utilization of the core(s) running KeepON PMD using *mpstat* by varying the batch size and slot size, under single-clock and dual-clock settings. We measure the average CPU utilization for 60 seconds and consider an idle background traffic scenario. We fix the slot size to 300 bytes when varying the batch size, and fix the batch size to 1 when varying the slot size.

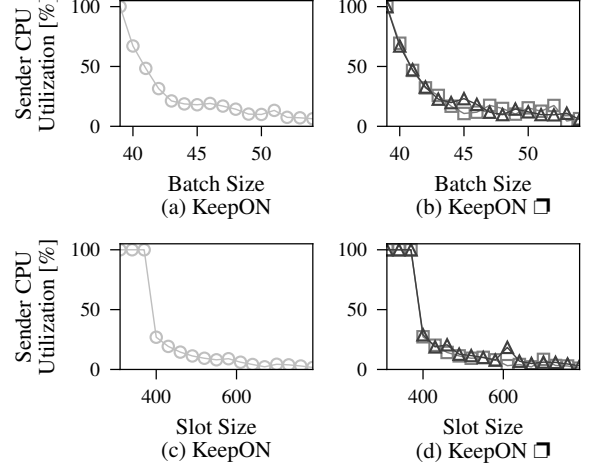


**Figure 19.** Sender CPU utilization of KeepON's CP-PMD as a function of batch size and slot size. CPU utilization was measured using *mpstat* with the system under idle state.

**Batch Size.** 1) *Single clock*: As shown in Figure 19(a), CPU utilization is highly dependent on the batch size. When the batch size is smaller than 39, the PMD core runs at nearly 100% utilization. As the batch size increases, allowing more packets to be processed per cycle, the utilization drops significantly, and eventually drops to 6.3% for batch sizes larger than 54; 2) *Dual clock*: As shown in Figure 19(b), two cores are involved for both TX and RX polling. Both cores exhibit a similar trend to the single-clock mode. With batch sizes smaller than 39, both cores are fully utilized (100% and 100%). The utilization decreases as batch size increases, dropping to 6.4% and 5.7% at a batch size of 54.

**Slot Size.** 1) *Single clock*: As shown in Figure 19(c), the slot size also has a substantial impact on CPU utilization. The PMD core reaches 100% utilization with small slot sizes ( $\leq 370$  bytes). Utilization substantially drops with larger slots (e.g., 26.92% at 400 bytes), eventually stabilizing (1.66% at 790 bytes); 2) *Dual clock*: Under the dual-clock configuration (Figure 19(d)), both PMD cores follow this pattern: full utilization at smaller slot sizes (100% at 370 bytes), with load decreasing as slot size increases and reduces processing overhead. This experiment shows that the CPU overhead of PMD

is highly sensitive to both batch size and slot size parameters. Properly tuning these parameters (e.g., using a batch size of at least 54 or a slot size of 670 bytes) significantly reduces the CPU cycles consumed by the PMD operations, resulting in minimal additional processing overhead.

### 7.5 Energy and Thermal Efficiency

We evaluate the energy efficiency of KeepON by monitoring its power consumption under different experimental settings. As shown in Figure 20, the original GENET driver exhibits a lower idle power consumption of approximately 1.9 W, which then scales with the traffic load, reaching up to 4.6 W at 1 Gbps. In contrast, KeepON's power profile is highly dependent on the polling parameter settings. Under non-optimized settings (Figure 20(a)(c)), such as a small batch size of 20 or a small packet size of 500 bytes, KeepON exhibits a significantly higher idle power consumption of approximately 3.4 W. However, the power consumption remains relatively stable as the bandwidth increases. By optimizing the polling parameters (Figure 20(b)(d)), such as increasing the batch size to 40 or the packet size to 1500 bytes, KeepON's idle power is reduced to 2.7 W, and KeepON becomes more energy-efficient than GENET at target bandwidths exceeding approximately 300 Mbps. This demonstrates that while KeepON's polling-based mechanism inherently consumes more power in an idle state, it becomes more efficient under high network loads by avoiding the significant overhead of frequent interrupts. Furthermore, this advantage is maximized through careful tuning of its PMD parameters.

We also compared the thermal impact of KeepON and the original GENET driver. Figure 22 shows CPU temperatures over time for GENET, a high-stress PMD KeepON configuration, and an optimized KeepON setup. The unoptimized KeepON (slot size = 300 byte, batch size = 1) stabilized CPU temperatures at 54-56°C, significantly higher than GENET's 43-45°C, illustrating the thermal cost of aggressive polling for determinism. However, optimizing PMD settings (slot size = 1500, batch size = 32) in KeepON (Optimized) improved thermal efficiency, maintaining a lower 47-49°C. These results show that carefully tuned PMD parameters allow KeepON's energy efficiency to approach GENET's while preserving deterministic communication.

## 8 Case Study

To further evaluate the applicability and effectiveness of KeepON, we conduct a case study in a multi-hop network environment by integrating KeepON in a TSN testbed.

**Testbed Setup.** The TSN testbed, as shown in Figure 21(a), consists of four TTEch FPGA-based network bridges (③), four KeepON-enabled end devices implemented on RPi 4B (①). A Central Network Controller (CNC), running on a PRi 4B (④), is responsible for schedule computation and distribution. To measure performance with high fidelity, a

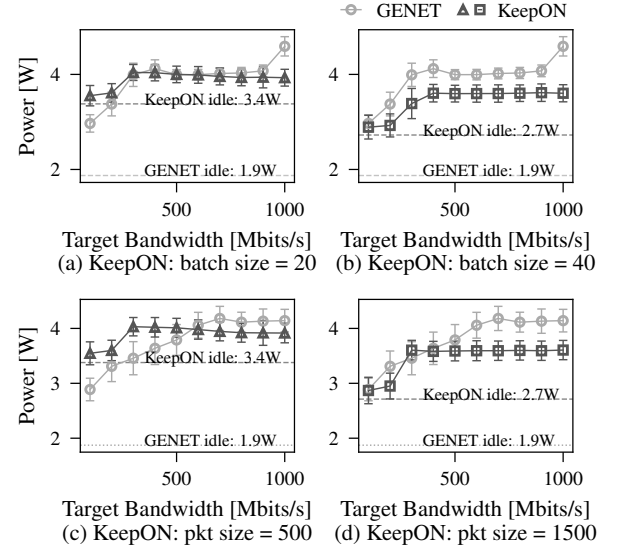


**Figure 20.** Power consumption comparisons of KeepON and GENET under different settings.

dedicated listener device, a RPi CM4 equipped with an Intel i210 NIC (②), utilizes hardware timestamping to accurately capture the end-to-end delay and jitter of received packets.

**Experimental Settings.** The network topology, shown in Figure 21(b), consists of four TSN bridges interconnected in a ring, and the four end devices generate a total of 12 distinct traffic flows. Each flow consists of uniform 64-byte packets and is randomly assigned a period of 4, 8, 16, or 32 ms, indicating a 32-ms hyperperiod of all the flows. To analyze the performance of each flow individually, we run all the flows but only measure one flow at a time using the dedicated RPi CM4 listener. The TSN schedule is configured with a uniform time slot of 16  $\mu$ s, a value chosen to meet the switch hardware's 320 ns granularity requirement. The KeepON PMD's slot size is set to 1250 bytes, which pads each 64-byte packet to a consistent on-wire transmission time of 1  $\mu$ s. We set the isolation of the ring buffer based on each flow's period and offset, ensuring each flow's packets are transmitted following the global TSN schedule.

**Single-hop Results.** Figure 21(d) shows the end-to-end jitters for a traffic flow from Talker (implemented with KeepON, IGB, and GENET) to Listener across single TSN switch. KeepON and IGB exhibit significantly lower jitter, with median absolute jitters of 4 ns and 5 ns, respectively. In contrast, GENET shows a median absolute jitter of 14.3  $\mu$ s. Furthermore, with KeepON and IGB, fewer than 1% of the packets fail to arrive within pre-allocated time window, where GENET has a 27.7% failure rate that packets from end devices do not align their schedule on TSN switch. In Figure 21(e), we compare the synchronization precision of the three methods from the grandmaster clock. One can observe that KeepON achieves

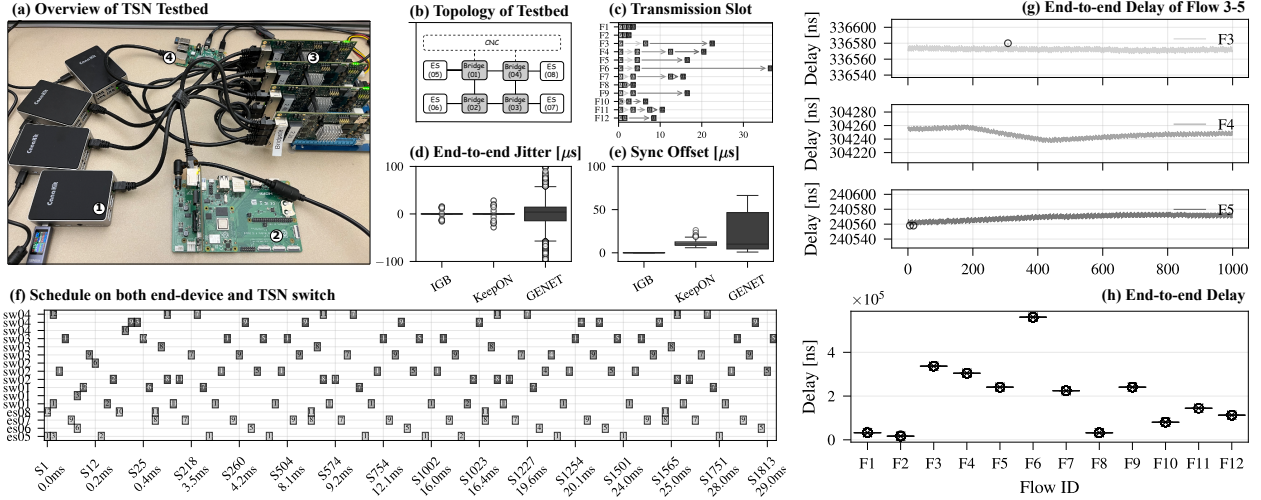


**Figure 21.** Performance evaluation of KeepON on a TSN testbed. (a) Overview of the testbed comprising four TSN bridges and four end devices. (b) Network ring topology; (c) Flow transmission time decided by the TSN schedule; (d) Single-hop end-to-end jitter comparison; (e) PTP synchronization offset from TSN grandmaster clock; (f) Global TSN schedule showing allocated transmission windows on both end devices and TSN bridges; (g) Time-series measurements of end-to-end delay for representative flows F3-F5; (h) Overview of measured end-to-end delays for all 12 flows.

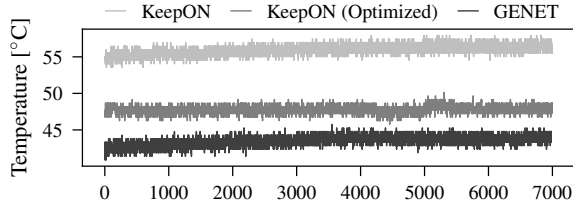


**Figure 22.** CPU thermal status comparisons.

a median absolute offset of  $10.3\mu\text{s}$ . While this is less precise than IGB ( $0.05\mu\text{s}$ ), its performance is almost the same as the default software PTP stack ( $10.07\mu\text{s}$ ). Notably, KeepON demonstrates a significantly tighter synchronization bound ( $25.8\mu\text{s}$ ) compared to GENET ( $56.2\mu\text{s}$ ). The observed synchronization degradation compared to back-to-back measurement is likely stems from configuration constraints imposed by the TSN switch’s GM: 1) A high PTP synchronization message interval ( $2^{-3}$  sec compared with 1 sec in our setting) may delay synchronization processing under KeepON’s limited bandwidth; 2) Layer 2 PTP enforced by bridge implementation (vs. Layer 4 in our evaluations) necessitated large KeepON slot sizes due to lack of fragmentation; 3) Multi-hop distances to the grandmaster clock can inherently reduce synchronization precision.

**Multi-hop Results.** We measure the end-to-end delay and jitter performance of 12 traffic flows traversing the multi-hop TSN testbed. Each flow is analyzed individually under full network load conditions to isolate path-specific performance characteristics. Our measurements reveal that KeepON successfully maintains deterministic timing behavior across all

flows, with end-to-end delays closely matching the expected values computed from the TSN schedule.

Figure 21(g) presents the end-to-end delay measurements for all 12 flows. The flows exhibit three distinct delay profiles corresponding to their path lengths in the ring topology. Short-path flows (F1, F2, F8) demonstrate mean delays between  $16\text{--}33\mu\text{s}$ , while the delay of medium-path flows (F10, F11, F12) ranges from  $80\text{--}144\mu\text{s}$ , and long-path flows (F3-F7, F9) exhibit delays of  $224\text{--}560\mu\text{s}$ . Notably, all flows maintain tight delay bounds with standard deviations below 25 ns, indicating stable and predictable performance. The measured mean delays closely align with the expected transmission times shown in Figure 21(c), with deviations typically less than 1% from the scheduled values. For instance, Flow 1 achieves a mean delay of  $32,568.5$  ns against an expected  $32,544$  ns (deviation of 0.075%).

The sub-microsecond jitter performance across all flows demonstrates KeepON’s ability to maintain deterministic timing in a multi-hop environment. As shown in Figure 21(e), flows F3-F5 exhibit consistent nanosecond-scale timing accuracy, with F4 and F5 showing minor drift patterns attributable to the clock drift ratio between talker and listener in PTP synchronization. Despite this drift, the total delay variation remains minimal, spanning only 54 ns for F4 and 46 ns for F5, confirming KeepON’s deterministic behavior.

Figure 21(f) illustrates the coordinated transmission schedule across end devices and TSN bridges, demonstrating how KeepON aligns packet transmissions with the global TSN schedule. The measured delays confirm that packets traverse their designated time slots at each hop, validating KeepON’s integration with the TSN control plane. This precise schedule

adherence enables the coexistence of flows with different periods (4, 8, 16, and 32 ms) within the same 32 ms hyperperiod without timing conflicts.

## 9 Conclusion

This paper presents KeepON, a novel software-based solution supporting deterministic traffic on end devices equipped with standard NICs. At its core, KeepON driver model integrates three key components, including Continuous-Pacing PMD, Emulated PTP Hardware Clock, and Scheduled Packet Insertion, to achieve precise and deterministic traffic scheduling. To extend support for end-to-end determinism for heterogeneous traffic types, we further propose two additional modules: Synchronization module and Traffic Management module. Moreover, we design a dual-clock approach by enabling two-directional linerate throughput to further improve synchronization performance. Extensive evaluations of our prototype, including integration with a TSN testbed, demonstrate that KeepON outperforms standard drivers and achieves performance comparable to hardware-based solutions. These results mark a significant step toward enabling deterministic communication on commodity platforms, offering a more flexible and accessible path to deploying deterministic networking in real-world systems.

## References

- [1] 2016. IEEE Standard for Local and metropolitan area networks – Bridges and Bridged Networks - Amendment 25: Enhancements for Scheduled Traffic. *IEEE Std 802.1Qbv-2015* (2016). <https://doi.org/10.1109/IEEESTD.2016.8613095>
- [2] 2020. Time and phase synchronization aspects of packet networks. <https://www.itu.int/rec/t-rec-g.8271/en> Series G: Transmission systems and media, digital systems and networks.
- [3] 2023. Intel Ethernet Controller I225 Series - Product Documents. <https://www.intel.com/content/www/us/en/products/details/ethernet/gigabit-controllers/i225-controllers/docs.html>.
- [4] Albert Gran Alcoz, Alexander Dietmüller, and Laurent Vanbever. 2020. {SP-PIFO}: Approximating {Push-In} {First-Out} behaviors using {Strict-Priority} queues. In *17th USENIX Symposium on Networked Systems Design and Implementation (NSDI 20)*. 59–76.
- [5] Clark Barrett, Roberto Sebastiani, Sanjit A Seshia, and Cesare Tinelli. 2021. Satisfiability modulo theories. In *Handbook of satisfiability*. IOS Press, 1267–1329.
- [6] Marcin Bosk, Filip Rezabek, Kilian Holzinger, Angela Gonzalez Marino, Abdoul Aziz Kane, Francesc Fons, Jörg Ott, and Georg Carle. 2022. Methodology and infrastructure for TSN-based reproducible network experiments. *IEEE Access* 10 (2022).
- [7] Alex Brinkman, Justin Morris, Irene Chen, Nabeel Sheikh, and Patrick Warren. 2021. Fastcat: an open-source library for composable Ethernet control systems. In *2021 IEEE Aerospace Conference (50100)*. 1–8.
- [8] James Coleman, Sara Almalih, Alexander Slota, and Yann-Hang Lee. 2019. Emerging cots architecture support for real-time TSN ethernet. In *Proceedings of the 34th ACM/SIGAPP Symposium on Applied Computing*.
- [9] Xiaotian Dai, Shuai Zhao, Yu Jiang, Xun Jiao, Xiaobo Sharon Hu, and Wanli Chang. 2020. Fixed-priority scheduling and controller co-design for time-sensitive networks. In *Proceedings of the 39th International Conference on Computer-Aided Design*. 1–9.
- [10] Leonardo De Moura and Nikolaj Bjørner. 2008. Z3: An efficient SMT solver. In *International conference on Tools and Algorithms for the Construction and Analysis of Systems*.
- [11] Josef Dorr, Karl Weber, and Steven Zupuncic. 2018. *Use Cases IEC/IEEE 60802*.
- [12] Paul Emmerich, Sebastian Gellenmüller, Daniel Raumer, Florian Wohlfart, and Georg Carle. 2015. Moongen: A scriptable high-speed packet generator. In *Proceedings of the 2015 Internet Measurement Conference*. 275–287.
- [13] Paul Emmerich, Maximilian Pudelko, Simon Bauer, and Georg Carle. 2018. User space network drivers. In *Proceedings of the 2018 Applied Networking Research Workshop*. 91–93.
- [14] Dario Faggioli, Juri Lelli, Claudio Scordino, and Luca Abeni. 2014. SCHED\_DEADLINE Scheduling in the Linux Kernel. <https://docs.kernel.org/scheduler/sched-deadline.html> Earliest Deadline First scheduler with Constant Bandwidth Server, available since Linux 3.14.
- [15] Norman Finn. 2018. Introduction to time-sensitive networking. *IEEE Communications Standards Magazine* 2, 2 (2018).
- [16] Daniel Firestone, Andrew Putnam, Sambhrama Mundkur, Derek Chiou, Alireza Dabagh, Mike Andrewartha, Hari Angepat, Vivek Bhanu, Adrian Caulfield, Eric Chung, et al. 2018. Azure accelerated networking: {SmartNICs} in the public cloud. In *15th USENIX Symposium on Networked Systems Design and Implementation (NSDI 18)*. 51–66.
- [17] Wolfgang Fischer, Joseph Gelish, and Michael Hegarty. 2021. *Aerospace TSN use cases, traffic types, and requirements*.
- [18] Thomas Frühwirth, Wilfried Steiner, and Bernhard Stangl. 2015. TTEthernet SW-based end system for AUTOSAR. In *10th IEEE International Symposium on Industrial Embedded Systems (SIES)*. IEEE, 1–8.
- [19] Alexej Grigorjew, Philip Diederich, Tobias Hofffeld, and Wolfgang Kellerer. 2022. Affordable Measurement Setups for Networking Device Latency with Sub-Microsecond Accuracy. (2022).
- [20] Jinho Hwang, K K Ramakrishnan, and Timothy Wood. 2015. NetVM: High performance and flexible networking using virtualization on commodity platforms. *IEEE Transactions on Network and Service Management* 12, 1 (2015), 34–47.
- [21] ieee. 2020. IEEE Standard for a Precision Clock Synchronization Protocol for Networked Measurement and Control Systems. *IEEE Std 1588-2019 (Revision of IEEE Std 1588-2008)* (2020), 1–499. <https://doi.org/10.1109/IEEESTD.2020.9120376>
- [22] ieee. 2022. IEEE Standard for Ethernet. *IEEE Std 802.3-2022 (Revision of IEEE Std 802.3-2018)* (2022), 1–7025. <https://doi.org/10.1109/IEEESTD.2022.9844436>
- [23] Intel Corporation. 2023. *Intel Ethernet Controller I210 Datasheet*. [https://cdrdv2-public.intel.com/333016/333016-I210\\_Datasheet\\_v\\_3\\_7.pdf](https://cdrdv2-public.intel.com/333016/333016-I210_Datasheet_v_3_7.pdf) Revision 3.7.
- [24] Eleftherios Kyriakakis, Maja Lund, Luca Pezzarossa, Jens Sparsø, and Martin Schoeberl. 2020. A time-predictable open-source TTEthernet end-system. *Journal of Systems Architecture* (2020).
- [25] Ao Li and Ning Zhang. 2024. Data-flow availability: Achieving timing assurance in autonomous systems. In *18th USENIX Symposium on Operating Systems Design and Implementation (OSDI 24)*. 445–463.
- [26] Chenglong Li, Zonghui Li, Tao Li, Cunlu Li, and Baosheng Wang. 2023. A Deterministic Embedded End-system Tightly Coupled with TSN Schedule. *IEEE Transactions on Computer-Aided Design of Integrated Circuits and Systems* (2023).
- [27] Linux Foundation Real-Time Project. 2024. PREEMPT\_RT Real-Time Linux Kernel Patches. <https://wiki.linuxfoundation.org/realtime/start> Real-time patches for Linux kernel, merged into mainline kernel 6.12.
- [28] Michael M Madden. 2019. Challenges using the Linux network stack for real-time communication. In *AIAA Scitech 2019 Forum*. 0503.
- [29] Anna Minaeva and Zdeněk Hanzálek. 2021. Survey on periodic scheduling for time-triggered hard real-time systems. *ACM Computing Surveys (CSUR)* 54, 1 (2021), 1–32.



- [30] Naresh Ganesh Nayak, Frank Dürr, and Kurt Roethermel. 2016. Time-sensitive software-defined network (TSSDN) for real-time applications. In *Proceedings of the 24th International Conference on Real-Time Networks and Systems*. 193–202.
- [31] Rolf Neugebauer, Gianni Antichi, José Fernando Zazo, Yury Audzevich, Sergio López-Buedo, and Andrew W Moore. 2018. Understanding PCIe performance for end host networking. In *Proceedings of the 2018 Conference of the ACM Special Interest Group on Data Communication*. 327–341.
- [32] NVIDIA Corporation. 2024. *Accurate Scheduling - NVIDIA 5T Technology User Manual v1.0*. NVIDIA. <https://docs.nvidia.com/networking/display/nvidia5ttechnologyusermanualv10/accurate+scheduling> Accessed: 2024.
- [33] Description of Converged Traffic Types Industry IoT Consortium. 2019. *time sensitive networks for flexible manufacturing testbed characterization and mapping of converged traffic types*.
- [34] Wei Quan, Wenwen Fu, Jinli Yan, and Zhigang Sun. 2020. OpenTSN: an open-source project for time-sensitive networking system development. *CCF Transactions on Networking* 3 (2020).
- [35] Sivasankar Radhakrishnan, Yilong Geng, Vimalkumar Jeyakumar, Abdul Kabbani, George Porter, and Amin Vahdat. 2014. {SENIC}: Scalable {NIC} for {End-Host} rate limiting. In *11th USENIX Symposium on Networked Systems Design and Implementation (NSDI 14)*. 475–488.
- [36] Deepti Raghavan, Shreya Ravi, Gina Yuan, Pratiksha Thaker, Sanjari Srivastava, Micah Murray, Pedro Henrique Penna, Amy Ousterhout, Philip Levis, Matei Zaharia, et al. 2023. Cornflakes: Zero-copy serialization for microsecond-scale networking. In *Proceedings of the 29th Symposium on Operating Systems Principles*. 200–215.
- [37] Hugo Sadok, Nirav Atre, Zhipeng Zhao, Daniel S Berger, James C Hoe, Aurojit Panda, Justine Sherry, and Ren Wang. 2023. {Ensō}: A streaming interface for {NIC-Application} communication. In *17th USENIX Symposium on Operating Systems Design and Implementation (OSDI 23)*. 1005–1025.
- [38] Ahmed Saeed, Yimeng Zhao, Nandita Dukkipati, Ellen Zegura, Mostafa Ammar, Khaled Harras, and Amin Vahdat. 2019. Eiffel: Efficient and flexible software packet scheduling. In *16th USENIX Symposium on Networked Systems Design and Implementation (NSDI 19)*. 17–32.
- [39] Jesus Sanchez-Palencia and Vinicius Costa Gomes. 2023. *ETF - Earliest TxTime First*. The Linux Foundation. <https://man7.org/linux/man-pages/man8/tc-etf.8.html> Linux Traffic Control Manual.
- [40] Henry N Schuh, Arvind Krishnamurthy, David Culler, Henry M Levy, Luigi Rizzo, Samira Khan, and Brent E Stephens. 2024. CC-NIC: a Cache-Coherent Interface to the NIC. In *Proceedings of the 29th ACM International Conference on Architectural Support for Programming Languages and Operating Systems, Volume 1*. 52–68.
- [41] Naveen Kr Sharma, Chenxingyu Zhao, Ming Liu, Pravein G Kannan, Changhoon Kim, Arvind Krishnamurthy, and Anirudh Sivaraman. 2020. Programmable calendar queues for high-speed packet scheduling. In *17th USENIX Symposium on Networked Systems Design and Implementation (NSDI 20)*. 685–699.
- [42] Dawei Shen, Tianyu Zhang, Jiachen Wang, Qingxu Deng, Song Han, and Xiaobo Sharon Hu. 2022. QoS guaranteed resource allocation for coexisting eMBB and URLLC traffic in 5G industrial networks. In *2022 IEEE 28th International Conference on Embedded and Real-Time Computing Systems and Applications (RTCSA)*. IEEE, 81–90.
- [43] Emiliano Sisinni, Abusayeed Saifullah, Song Han, Ulf Jennehag, and Mikael Gidlund. 2018. Industrial internet of things: Challenges, opportunities, and directions. *IEEE transactions on industrial informatics* 14, 11 (2018), 4724–4734.
- [44] Livio Soares and Michael Stumm. 2010. {FlexSC}: Flexible system call scheduling with {Exception-Less} system calls. In *9th USENIX Symposium on Operating Systems Design and Implementation (OSDI)*.
- [45] Brent Stephens, Aditya Akella, and Michael Swift. 2019. Loom: Flexible and efficient {NIC} packet scheduling. In *16th USENIX Symposium on Networked Systems Design and Implementation (NSDI 19)*. 33–46.
- [46] William Tu, Yi-Hung Wei, Gianni Antichi, and Ben Pfaff. 2021. Revisiting the open vswitch dataplane ten years later. In *Proceedings of the 2021 ACM SIGCOMM 2021 Conference*. 245–257.
- [47] Marian Ulbricht, Stefan Senk, Hosein K Nazari, How-Hang Liu, Martin Reisslein, Giang T Nguyen, and Frank HP Fitzek. 2023. Tsn-flextest: Flexible tsn measurement testbed. *IEEE Transactions on Network and Service Management* 21, 2 (2023), 1387–1402.
- [48] Chuanyu Xue, Tianyu Zhang, and Song Han. 2024. Towards Cost-Effective Real-Time High-Throughput End Station Design for Time-Sensitive Networking (TSN). In *Proceedings of the 61st ACM/IEEE Design Automation Conference*. 1–6.
- [49] Chuanyu Xue, Tianyu Zhang, Yuanbin Zhou, Mark Nixon, Andrew Loveless, and Song Han. 2024. Real-Time Scheduling for 802.1Qbv Time-Sensitive Networking (TSN): A Systematic Review and Experimental Study. In *Proceedings of the 30th IEEE Real-Time and Embedded Technology and Applications Symposium*.
- [50] Chuanyu Xue, Tianyu Zhang, Yuanbin Zhou, Mark Nixon, Andrew Loveless, and Song Han. 2025. A Survey and Experimental Study of Real-Time Scheduling Methods for 802.1 Qbv TSN Networks. *Comput. Surveys* (2025).
- [51] Tianyu Zhang, Gang Wang, Chuanyu Xue, Jiachen Wang, Mark Nixon, and Song Han. 2024. Time-Sensitive Networking (TSN) for Industrial Automation: Current Advances and Future Directions. *Comput. Surveys* 57, 2 (2024), 1–38.
- [52] Tianyu Zhang, Chuanyu Xue, Jiachen Wang, Zelin Yun, Natong Lin, and Song Han. 2024. A survey on industrial Internet of Things (IIoT) Testbeds for connectivity research. *arXiv preprint arXiv:2404.17485* (2024).
- [53] Yang Zhou, Xingyu Xiang, Matthew Kiley, Sowmya Dharanipragada, and Minlan Yu. 2024. {DINT}: Fast {In-Kernel} Distributed Transactions with {eBPF}. In *21st USENIX Symposium on Networked Systems Design and Implementation (NSDI 24)*. 401–417.

## A Appendix

### A.1 Related Work

Existing works supporting deterministic communication on end devices can be broadly classified into hardware-dependent and hardware-independent solutions.

**Hardware-Dependent Solutions.** Several hardware-based approaches have been developed to enhance network performance and scheduling efficiency by leveraging specialized hardware features. For instance, SENIC [35] demonstrates scalable NIC rate limiting on NetFPGA. Loom [45] provides flexible NIC packet scheduling through hardware modifications to improve scheduling efficiency. Azure Accelerated Networking [16] demonstrates the production-scale deployment of FPGAs, achieving low VM-VM latencies and 32 Gbps throughput. Programmable Calendar Queues [41] enable time-aware priority escalation on programmable switches, such as Barefoot Tofino, for algorithms requiring dynamic packet priority changes. While these approaches significantly improve performance and scheduling flexibility, they focus on throughput optimization and average latency reduction rather than providing strict timing determinism.

There are several hardware-dependent solutions aim to achieve deterministic communication at end devices by leveraging specific hardware features, which provide highly precise scheduling and synchronization capabilities.

- *Specialized Platform.* One type of solution relies on FPGAs or specialized System-on-Chip (SoC). For instance, Quan et al. [34] propose an SDN-based TSN control mechanism using Xilinx FPGA with a novel management protocol. Kyriakakis et al. [24] present the design and implementation of a time-predictable TTEthernet end system based on the open-source Patmos processor. In [26], an open-source FPGA TSN end device implementation is proposed to support precise time-triggered task release. However, the specialized nature of these FPGA/SoC-based solutions limits their applicability and easy integration into existing systems.

- *General Systems with Specialized NICs.* Another common and more widely adopted hardware-dependent approach utilizes general-purpose operating systems (e.g., Linux) augmented with specialized NICs that support hardware offloading. In this thread of work, several research efforts have been conducted, focusing on improving delay, jitter, and system throughput [6, 8, 19]. Besides interacting via standard Linux APIs, some other works employ user-space frameworks, e.g., DPDK, to bypass kernel overhead and gain finer control [30, 48]. This approach is flexible since it leverages a standard OS and typically does not require extensive, ground-up development, making it cost-effective. However, it still requires specific NIC hardware, which is unavailable in legacy systems, and some embedded systems may not even have an available PCIe port to install such an extension NIC, such as Raspberry Pi and Arduino.

**Hardware-Independent Design** Several existing studies aim to reduce packet transmission latency at the network stack or OS level using hardware-independent techniques, including kernel bypass [20], accelerated eBPF/XDP processing [46, 53], and streamlined network stacks [37]. Recent software packet scheduling advances, such as Eiffel [38], which uses integer-based priority queues to achieve  $O(1)$  scheduling operations, and SP-PIFO [4], which approximates complex scheduling on commodity hardware, demonstrate significant efficiency improvements. However, these approaches focus on packet ordering (priority) rather than precise transmission time. Cornflakes [36] demonstrates microsecond-scale networking through zero-copy serialization techniques, achieving higher throughput compared to using pure software approaches. Although these methods are able to reduce average latency, they do not provide any guarantee of strict timing determinism.

Purely software-based approaches for deterministic communication remain rare and typically suffer from performance limitations compared to hardware solutions, largely due to inherent sources of random delay, as discussed in §1.

Although the Linux kernel provides software TSN mechanisms like TAPRIO and ETF for traffic shaping and scheduling (operable even without hardware offloading), their deterministic performance degrades significantly without using specialized NICs [39, 47]. The PREEMPT\_RT Linux kernel patches [27] provide a foundation for kernel-level real-time networking, achieving  $100\mu\text{s}$  worst-case scheduling latency, while SCHED\_DEADLINE offers EDF scheduling with temporal isolation for time-critical tasks [14]. Frühwirth et al. [18] propose a software-based TTEthernet end system that achieves  $30\mu\text{s}$  jitter for time-triggered transmissions. Similarly, Fastcat [7], an open-source C++ library for EtherCAT end devices using standard NICs, supports 1 kHz real-time communication but lacks evaluation of its deterministic performance and remains limited to 100 Mbps EtherCAT networks.

## A.2 Driver Implementation

**DMA Ring Initialization.** We initialize the driver by pre-allocating static packet buffers (skb) using `dev_alloc_skb` for all descriptors in the transmit DMA ring. These buffers all have the same fixed size (by the slot size parameter) and are initialized with corrupted CRC values. We create the consistent DMA mappings for these buffers using the streaming DMA API (`dma_map_single`) at startup. While this requires explicit synchronization before the NIC accesses the data (after CPU writes), we choose this over the `dma_alloc_coherent` API to have finer control and avoid cache coherency overhead associated with coherent buffers. Each descriptor has flags added to track its status and ownership (belonging to which traffic class). Initially, the NIC’s consumer/completion index is set to 0, and the driver’s producer index is set to batch size. We disable NIC interrupts and the NAPI subsystem for Tx, which is standard practice for polling-mode drivers (PMDs) to minimize PCIe transaction overhead and processing latency. Finally, a dedicated polling thread is created for transmit operations using `kthread_create_on_cpu`, ensuring it runs on a specific CPU core for minimum pre-emption.

**Identify Transmitted Packets.** Two approaches are generally available to determine when the NIC has finished transmitting packets. 1) The driver periodically reads a NIC register (via MMIO), which indicates how many descriptors the NIC has processed (e.g., a completion or consumer index). The driver compares this NIC index with its own record of submitted packets (its producer index) to identify completed transmissions. This method is simple and compatible with most standard NICs. 2) Some NICs update status directly within the descriptor memory itself, e.g., Intel i210/i225 using Descriptor Done (DD) bits, or others using Completion Queue Entries (CQEs) [3, 23]. The driver can poll this memory location, which involves less overhead compared to MMIO register reads, to check for completion

**Table 3.** Relative Throughput (%) under varying batch size and polling period ( $\mu$ s) settings. Packet size is 300 bytes.

Batch size	Polling-period [ $\mu$ s]			
	0	10	100	1000
1	99.99%	16.77%	2.18%	0.00%
8	100.00%	100.00%	18.31%	1.89%
64	100.00%	100.00%	100.00%	15.30%
512	100.00%	100.00%	100.00%	100.00%

flags. This can be more efficient, but requires specific NIC hardware support. In our implementation, we select the first approach (i.e., Index Comparison) for broader compatibility. Once the PMD identifies that a packet has been transmitted, we intentionally modify its CRC field in the buffer, setting it to  $0x00$  as corrupted, assuming a low probability of collision with any valid CRC needed. We use solution 1) in our prototype.

**Polling Period.** Our polling thread reclaims transmitted buffer descriptors in batches, controlled by the batch size parameter. The polling frequency (period) is critical for achieving stable line-rate performance without overwhelming the CPU. It must be fast enough to free up descriptors before the transmit ring fills. The polling period is determined by the packet transmission time (depending on PMD’s slot size) and the number of packets processed per poll (batch size). Specifically, the polling period must satisfy the following relationship to keep pace with the line rate: polling period  $\leq$  line-rate / (slot size  $\times$  batch size) - polling overhead. Here, polling overhead represents the worst-case time the driver takes to process one batch of completed packets. Table 3 validates parameter combinations (slot size and batch size) by measurements that satisfy this condition in the above equation and enable line-rate throughput. In practice, the polling thread uses `usleep_range(1b, ub)` to control polling period, yielding the CPU. We set the sleep range based on the calculated maximum polling period and use a pessimistic overhead value of 100  $\mu$ s in our implementation.

**Packet Insertion.** For packet insertion, the driver first obtains the target Tx ring descriptor index from the scheduler. The scheduler implements different insertion strategies based on traffic type:

- **Real-time Traffic:** For packets with `SO_TXTIME` timestamps, the scheduler calculates the target slot according to the scheduled transmission time. If the target slot is available and the packet arrived on time, it is placed in the target slot. Otherwise, the driver implementation supports two modes: (i) **Strict Mode** drops the packet to maintain hard real-time guarantees, and (ii) **Relaxed Mode** (used only when isolation is not aligned with schedule) finds the earliest available slot within the traffic class’s allocated slots, trading timing precision for higher delivery rates.

- **Best-effort Traffic:** Packets without timing constraints use any available slot not reserved for real-time traffic classes, ensuring they only utilize unreserved bandwidth.

After obtaining a valid slot index, the driver copies (`memcpy`) the packet data into a pre-allocated buffer on the transmit ring. A `dma_sync_single_for_device` call ensures the NIC observes the data by flushing cache, and the descriptor is marked as ready by setting its state flag. For PTP packets, the driver passes the scheduled timestamp to the kernel using `skb_tstamp_tx` for hardware timestamping. Since packet insertion operates in parallel with the polling mechanism, a spinlock protects the shared ring buffer from concurrent access.

**Dual Clock Mode.** In dual-clock mode, Continuous-Polling PMD creates another separate polling-based thread for the Rx path to avoid the interrupt overhead. Compared with the Tx polling mechanism, there is a timestamping problem on the Rx side, where the NIC drops corrupted packets directly in hardware (as discussed in Section 2). This means the software driver, operating in the polling Rx thread, only sees the genuine packets arriving in memory (i.e., the DMA ring). Because the dropped packets are invisible to the driver, it loses the original sequence of arrivals. While a hardware counter (e.g., `bcmgenet`’s `DMA_P_INDEX_DISCARD_CNT`) might report the number of dropped packets, the driver doesn’t know when they were dropped relative to the packets it received. This prevents accurate timestamping of the receiving packet as it initially hits the NIC. There are two potential solutions: 1) Disable the NIC’s hardware CRC check, forcing it to pass all packets (corrupted and genuine) to the driver, thus preserving the sequence for timestamping; 2) Use a smaller batch size when polling and timestamping, which could offer relatively improved accuracy. We pick the first one for dual-clock mode.

We identify two threats to the validity of the implementation of dual clock mode. 1) Even though the dual clock mode can achieve accurate time synchronization after it converges, the convergence time is unpredictable and can be up to several minutes. For example, Figure 23 shows a case where the single clock mode is synchronized within 5 seconds, but the dual clock mode takes more than 80 seconds. We believe this is due to the algorithm of the dual clock combination used to merge the Tx and Rx clocks. 2) We noticed that if we delay adding necessary padding data (discussed in Section 4.3) in reclaiming steps during PMD polling, it becomes harder to hit the line-rate target in dual-clock mode. This might be caused by cache pollution, where the two separate threads access the memory in an interleaved manner, leading to cache misses. Thus, for dual-clock mode, we add the padding on demand when it just reaches the driver.

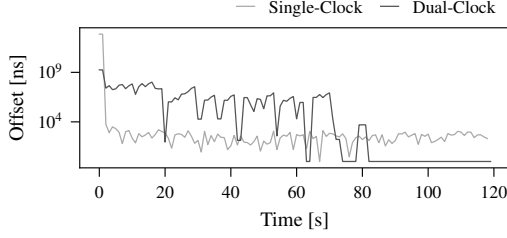


**Figure 23.** Convergence time of PTP synchronization of KeepON under Single-Clock vs. Dual-Clock mode.

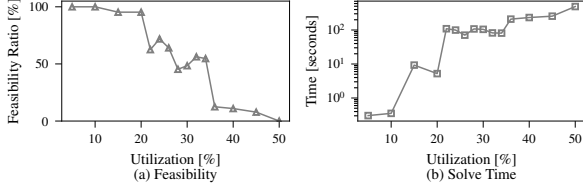


**Figure 24.** Schedulability analysis across utilization levels. (a) Percentage of flowsets with feasible isolation and schedules. (b) Average Z3 solving time showing exponential growth with utilization.

### A.3 System-Level Optimization

We use the line rate of 1 Gbps for all experiments, which is the maximum for RPi’s default NIC. We use the default energy governor, such as CPU frequency scaling and idle state power adaptation. We set the energy mode as on-demand for Figure 20 to observe true power consumption. We set the Linux socket buffer to a large value of 250MB to avoid potential packet loss. To reduce the impact of the system scheduler and accurately show how PMD parameters affect system performance, we isolate one or two cores to run the polling thread of KeepON for single-clock and dual-clock mode, respectively, affixing the PMD thread to each core. We disable the CPU periodic timer interrupt and IRQ for isolated cores. The single clock mode for KeepON is applied unless otherwise specified.

### A.4 Isolation Configuration

To evaluate the feasibility and tractability of our traffic isolation scheduling model, we conducted extensive simulation experiments using the Z3 SMT solver to analyze schedulability under varying real-time traffic loads.

**Experimental Setup.** We generate synthetic flowsets with system utilization ranging from 5% to 50%. The utilization is calculated as the ratio of total packet instances per ring cycle to the number of slots. Given each utilization value, we created 64 different flow configurations using the parameters summarized in Table 4.

**Z3 Scheduling Analysis.** For each flowset, we employed Z3 to determine whether a feasible partition  $\mathcal{F}$  and schedule  $\mathcal{S}_i$  exist that satisfy all constraints (in Section 6.1). The solver searches for slot allocations to traffic classes and transmission times within the hyperperiod, with a 150-second

**Table 4.** Flowset parameters for schedulability analysis

Parameter	Configuration
System utilization	{5%, 10%, 15%, ..., 50%}
Number of flows	{2, 4, 8, 12, 16}
Flow periods	{80, 160, 240, ..., 1600 $\mu$ s}
Max jitter	5 – 20% of flow period
Slot size	10 $\mu$ s
Ring size	32 slots
Traffic classes	$\leq 8$ classes
Datasets per experiment	64

timeout for complex instances. If the solver cannot find a feasible solution within the given time period limit, the flowset is considered infeasible. All flow periods are chosen as harmonic to ensure bounded hyperperiods.

**Results.** Figure 24 presents the schedulability results across 896 flowsets:

1) *Schedulability:* As shown in figure 24(a), the schedulability reaches almost 100% at low utilization (5-20%) and decreases sharply when the utilization is larger than 25%. This demonstrates that our isolation model effectively handles typical industrial real-time workloads while revealing the fundamental limits of static partitioning.

2) *Runtime:* As shown in figure 24(b), Z3 solving time increases exponentially (less than 0.5 seconds at 5% utilization and over 100 seconds at 40-50% utilization), reflecting the growing constraint complexity as the solution space becomes more constrained.

### A.5 PTP Performance Analysis

To further understand the synchronization performance, we analyze the maximum time offset between the master and slave clocks caused by inaccurate timestamping at a single hop. We consider two sources of timestamping uncertainty:

- 1) Random timestamping delay, i.e.,  $j_M^{in}$ ,  $j_M^{out}$ ,  $j_S^{in}$ , and  $j_S^{out}$ ;
- 2) Clock granularity, denoted as  $g_M$ , and  $g_S$ , representing the resolution of the master and slave clocks, respectively.

Below, we analyze the maximum offset inaccuracy ( $\delta_{TS}$ ) and maximum drift accumulation ( $\delta_{Drift}$ ) caused by potentially inaccurate timestamping.

• *Offset Inaccuracy:* The PTP slave corrects its clock based on the offset between the master and slave clocks. The offset is calculated as  $O = [(t_2 - t_1) - (t_4 - t_3)]/2$ , as shown in Fig. 11 (Ⓐ). Ideally, the corrected time matches the master’s time without any offset. In practice, inaccurate timestamping causes each timestamp to deviate from the true event time  $t_{i,est} = t_{i,true} + \epsilon_i$ . The error in this offset calculation is  $((\epsilon_2 - \epsilon_1) - (\epsilon_4 - \epsilon_3))/2$ .

The error range for each timestamp is based on its granularity and jitter. That is:

$$\begin{aligned} \epsilon_1 &\in \left[-\frac{1}{2}g_M, \frac{1}{2}g_M + j_M^{out}\right] & \epsilon_2 &\in \left[-\frac{1}{2}g_S, \frac{1}{2}g_S + j_S^{in}\right] \\ \epsilon_3 &\in \left[-\frac{1}{2}g_S, \frac{1}{2}g_S + j_S^{out}\right] & \epsilon_4 &\in \left[-\frac{1}{2}g_M, \frac{1}{2}g_M + j_M^{in}\right] \end{aligned} \quad (3)$$

The maximum absolute value of the offset calculation error, which represents the uncertainty in the offset correction applied by the slave, can then be bounded by:

$$\delta_{TS} = \frac{1}{2} \left( g_M + g_S + \max \left( j_M^{in} + j_M^{out}, j_S^{in} + j_S^{out} \right) \right) \quad (4)$$

• **Drift Accumulation:** Even with frequency correction (②), a residual frequency error persists due to timestamp errors in frequency ratio estimation. The frequency ratio is estimated as  $(t_1^{next} - t_1)/(t_2^{next} - t_2)$ , and the measured ratio caused by timestamp errors is:

$$r_{meas} = \frac{\Delta t_M + \epsilon_M}{\Delta t_S + \epsilon_S} \quad (5)$$

where  $\epsilon_M \in [-(g_M + j_M^{out}), g_M + j_M^{out}]$  and  $\epsilon_S \in [-(g_S + j_S^{in}), g_S + j_S^{in}]$  represent the timestamp error differences between consecutive sync messages.

After frequency correction using  $r_{meas}$ , the residual frequency difference is  $\Delta\rho = \rho_S(r - r_{meas})$ , where  $r = \rho_M/\rho_S$  is the true ratio. The worst-case drift occurs when  $r_{meas}$  deviates maximally from  $r$ . For synchronized clocks where  $\Delta t_M \approx \Delta t_S \approx I$ , the maximum drift over interval  $I$  is:

$$\begin{aligned} \delta_{Drift} &= I \times \max(|\Delta\rho_{max}|, |\Delta\rho_{min}|) \\ &= I \times \rho_M \times \max \left[ \frac{g_S + j_S^{in}}{I - g_S - j_S^{in}}, \frac{g_M + j_M^{out}}{I + g_S + j_S^{in}} \right] \end{aligned} \quad (6)$$

The first term represents drift from overestimating the frequency ratio when master timestamps have positive errors and slave timestamps have negative errors, while the second term represents underestimation.

**Simulation Results.** To validate our theoretical analysis, we implement a PTP synchronization simulator with the following settings: a synchronization interval of 100 ms, a symmetric network delay of 10  $\mu$ s, and a 1 ppm frequency offset between the master and slave clocks in initialization. We use moving average window size 10 to smooth the frequency in simulation. Figure 25 shows the impact of timestamping jitter and clock granularity (decided by slot-size) on synchronization performance. As shown in Figure 25(a,c), clock granularity increases from 0.8 to 12  $\mu$ s, both offset and drift errors grow linearly, with median offset errors increasing from 0.5 to 2.7  $\mu$ s as 5.4 $\times$  increase. As shown in Figure 25(b,d), jitter has a more pronounced effect that its offset error increases from 0.03 to 1.5  $\mu$ s by 50 $\times$ , demonstrating that jitter has more impact on synchronization accuracy.

It is worth noting that our analysis result bounds the maximum drift within a single synchronization interval but does

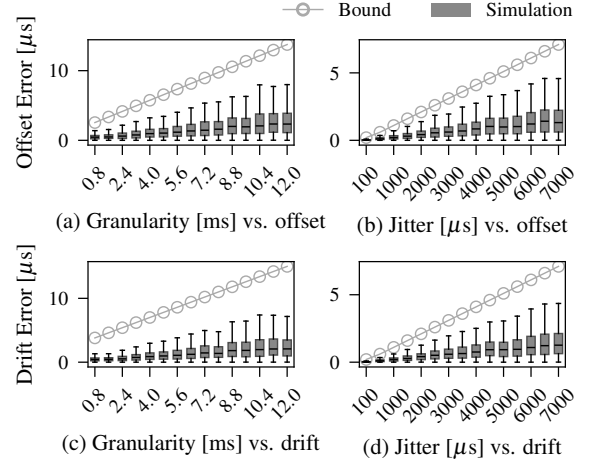


**Figure 25.** Impact of timestamp error parameters on PTP synchronization accuracy in simulation.

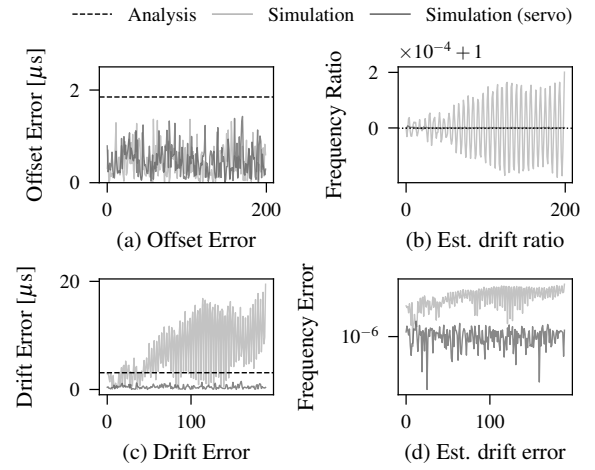


**Figure 26.** Comparison of PTP synchronization in simulation with and without frequency filtering.

not account for this multi-interval accumulation effect. Figure 26(b,c,d) grey line simulates a common limitation in PTP's drift correction that the estimated frequency ratio oscillates randomly due to random timestamping delay, which eventually causes drift errors to grow unbounded. To address this accumulation, many real PTP implementations apply different servo algorithms to filter the frequency ratio estimate. In our simulation, we implemented a simple 10-sample moving average filter to smooth the frequency. With filtering (black line in Figure 26(b,c,d)), the frequency ratio converges smoothly to the true value, reducing average drift errors by 12.2 $\times$  and keeping them near the single-interval bound. This demonstrates that while the theoretical analysis accurately predicts per-interval errors, practical implementations require frequency filtering to prevent the random walk accumulation that occurs over multiple synchronization cycles.

## A.6 API Design

We implement the Synchronization module and the Traffic Management module with existing Linux APIs to provide easy-to-use interfaces for seamless integration.

**Timestamp delivering.** To keep the compatibility with existing Linux APIs, we use the standard `SO_TXTIME` socket option to deliver the scheduled transmission time from userspace, as shown in Listing 1. The socket option conveys the desired timestamp via control messages `CMSG` within the `sendmsg` call, and the driver can parse the timestamp from the kernel’s socket buffer (`skb`) structure.

```
// Enable SO_TXTIME socket option
setsockopt(fd, SOL_SOCKET, SO_TXTIME, &sk_txtime,
sizeof(sk_txtime));

// Set scheduled time in CMSG
cmsg = CMSG_FIRSTHDR(&msg);
cmsg->cmsg_level = SOL_SOCKET;
cmsg->cmsg_type = SO_TXTIME;
cmsg->cmsg_len = CMSG_LEN(sizeof(__u64));
*((__u64 *) CMSG_DATA(cmsg)) = txtime;

// Send message
ret = sendmsg(fd, &msg, 0);
```

**Listing 1.** API: Example of userspace application to enable `SO_TXTIME` socket option and send scheduled packet.

**Pre-Buffering.** We utilize the queuing discipline (`qdisc`) framework in the Linux Traffic Control (TC) subsystem to implement traffic pre-buffering and prioritization [39]. First, we use the `mqprio` `qdisc` to create multiple logical traffic classes depending on the number of applications. While `mqprio` maps traffic classes to multiple hardware queues, in our configuration, these logical classes are mapped to partitions (§6.1) of a single hardware queue. Listing 2 shows an example: *1) For real-time traffic:* (e.g., 1:3 and 1:4), we attach an Earliest Time First (`etf`) `qdisc` to each respective class. This `qdisc` buffers packets and dequeues them based on their `SO_TXTIME` timestamp, which is set by the application to indicate the desired transmission time. The `etf` `qdisc` uses an efficient data structure, often a red-black tree, for ordering packets by their release time. The `delta` parameter specifies an offset before the packet’s scheduled timestamp when it should be released to the network driver. This accounts for worst-case packet transmission latencies, e.g., caused by system jitter and batching effects. *2) For best-effort traffic:* (e.g., traffic mapped to parents such as 1:1 and 1:2 in a four-class setup), a standard `pifo` `qdisc` is attached to each of these classes. This `qdisc` provides basic queuing without prioritization beyond the initial class assignment, ensuring that packets in the order they are received within their class.

**Synchronization.** To integrate with standard Linux time synchronization mechanisms, our driver exposes its EPHC capabilities through the PTP Hardware Clock (PHC) kernel API. This creates character devices in the `/dev/` directory (e.g., `/dev/ptp0`, `/dev/ptp1`), allowing userspace tools

```
## Application 0-7 use class 0, 8 use class 1
## 9-11 use class 2, 12-15 use class 3
sudo tc qdisc add dev eth0 root handle 1: mqprio
num_tc 4 \
    map 0 0 0 0 0 0 0 1 2 2 2 2 3 3 3 3 \
    queues 1@0 1@1 1@2 1@3 \
    hw 0

## Set class 1-2 as FIFO qdisc
sudo tc qdisc replace dev eth0 parent 1:1 pifo
sudo tc qdisc replace dev eth0 parent 1:2 pifo

## Set class 3-4 as ETF qdisc
sudo tc qdisc replace dev eth0 parent 1:3 etf
clockid CLOCK_TAI delta 50000
sudo tc qdisc replace dev eth0 parent 1:4 etf
clockid CLOCK_TAI delta 50000
```

**Listing 2.** API: Example for pre-buffering set up by Linux `Qdisc`.

to access and control these hardware clocks. The specific `/dev/ptpX` device corresponding to the network interface’s timestamps (e.g., a Tx-EPHC in single-clock setup or a combined-EPHC in dual-clock setup) is used by the PTP demon for internal or external synchronization. Listing 3 shows a typical synchronization setup with default settings.

- `phc2sys` synchronizes the system clock (e.g., `CLOCK_REALTIME`) to the internal PTP hardware clock (`/dev/ptpX`).
- `ptp4l` implements the IEEE 1588 PTP protocol to synchronize the hardware clock (`/dev/ptpX`) with an external PTP clocks over the network.

```
# Master
sudo phc2sys -s /dev/ptp0 -o 0 -m
sudo ptp4l -i eth0 -m -P

# Slave
sudo phc2sys -s /dev/ptp0 -o 0 -m
sudo ptp4l -i eth0 -m -P -s -p /dev/ptp1
```

**Listing 3.** API: Example of synchronization setup.

**Driver Parameters.** KeepON driver’s PMD behaviors can be configured through module parameters during initialization. Key parameters include:

- `slot_masks`: Specifies slot allocation for each traffic class using bitmasks. Each bit represents a slot in the fix-size (by default 32) ring buffer. For example, Listing 4 allocates slot 0 to class 0 and slots 1,17 to class 1, with the pattern repeating every 3.2ms cycle (32 slots  $\times$  100 $\mu$ s).
- `pkt_size`: Sets the slot size in bytes (up to 1518). This determines the line-rate packet transmission time.
- `batch_size`: Controls how many descriptors the polling thread processes per iteration (1-512), affecting CPU efficiency and synchronization performance.

```
# Load driver with two real-time classes
sudo insmod genet.ko slot_masks=0x01,0x20002,0,0,0
pkt_size=1230 batch_size=8
```

**Listing 4.** API: Example of loading KeepON driver.